UNIVERSITÉ LAVAL

THE USE OF FLUORESCENT BACTERIOPHAGES TO STUDY VIROAEROSOL CHARACTERISTICS

Mémoire

LOUIS GENDRON

Maîtrise en Biophotonique
Maître ès sciences (M.Sc.)

Québec, Canada

Résumé

Pour bien comprendre et contrôler les aérosols contenant des virus (viroaérosol), un modèle de laboratoire approprié est requis. Pour cette étude, trois bactériophages : P008 couplé au SYBR Gold, PP01 exprimant la GFP et λ exprimant la EYFP ont été comparés entre eux et à des microsphères fluorescentes non-biologiques pour leur potentiel en tant que modèle de laboratoire en aérovirologie. Les modèles viraux ont été aérosolisés à partir d'un tampon de phage en utilisant un nébuliseur de TSI (modèle 9301) connecté à une chambre d'aérosols. La taille aérodynamique des aérosols ainsi que leur distribution ont été déterminées à l'aide d'un spectromètre de particules aérodynamique (APS, TSI modèle 3321). Les échantillons de viroaérosols ont été capturés à l'aide d'un impacteur Andersen à six étages contenant soit du tampon de phage à l'intérieur des plaques de chaque étage ou un milieu solide (agar à 1.5%). Les techniques des plages de lyse, du qPCR et la microscopie à fluorescence ont été utilisées pour quantifier les virus récupérés sur les étages de l'impacteur. La microscopie à fluorescence a aussi été utilisée pour quantifier et analyser les modèles viraux sur des particules seules et sur milieu solide. L'ADN viral, des plages de lyse ainsi que des particules fluorescentes ont été observées sur les étages 3 à 6 de l'échantillonneur ce qui corrélait avec les données obtenues par l'APS. La microscopie à fluorescence a permis de visualiser les modèles viraux sur ou à l'intérieur des particules d'aérosols. Ces résultats confirment que les virus peuvent être présents dans l'atmosphère sous forme d'aérosol dont la dimension est bien plus grande que celle de leur propre taille, et que les virus en aérosol peuvent être quantifiés et observés en utilisant la microscopie à fluorescence. L'ensemble de ces résultats suggèrent qu'un bactériophage fluorescent serait un excellent modèle de laboratoire pour étudier le comportement des virus dans l'air.

Abstract

In order to understand and control virus aerosols (viroaerosols), an appropriate laboratory model is required. In this study, fluorescent bacteriophages P008 coupled to SYBR Gold, PP01 expressing GFP and λ expressing EYFP were compared to non-biological fluorescent microspheres for their potential as viral models in aerovirology. The test viruses were aerosolized in phage buffer using TSI's 9301 model atomizer attached to a commercially available aerosol chamber. The aerodynamic particle size distribution of the viroaerosols was determined with an aerodynamic particle sizer (APS, TSI's 3321 model). Samples were collected with a Six-stage Andersen impactor loaded with Petri dishes containing either phage buffer or a solid 1.5% agar medium. Plaque assays, qPCR and fluorescence microscopy were used to quantify the virus load on each stage of the impactor. Fluorescence microscopy was also used to quantify and analyze single aerosol particles in liquid or solid media. Viral DNA, infectious particles and fluorescent particles were detected on stages 3 to 6 of the sampler and correlated with the aerodynamic particle distribution. Fluorescence microscopy permitted visualization of viruses on or encapsulated inside aerosol particles and on a solid medium. These results confirm that viruses may be present in the atmosphere as aerosols, which are much larger than their own particle size, and that viruses could be visualized and quantified in aerosols using fluorescence microscopy. These findings suggest that a fluorescence-expressing bacteriophage would be an excellent laboratory model for the study of viruses in aerosols.

Contents

List of Abbreviations

APS aerosol particle sizer

DAPI 4' 6-diamidino-2-phenylindole

dsDNA double-stranded deoxyribonucleic acid

EFM epi-fluorescence microscopy

ϵ molar absorption coefficient

η quantum yield

FCM flow cytometry

FITC Fluorescein isothiocyanate

FLIM fluorescence-lifetime imaging microscopy

GFP green fluorescent protein

MMAD mass median aerosol diameter

PFU plaque forming unit

qPCR quantitative polymerase chain reaction

qRT-PCR quantitative reverse-transcription polymerase chain reaction

RH relative humidity

RNA ribonucleic acid

RR Relative recovery

SARS severe acute respiratory syndrome

SOC small outer capsid

TEM transmission electron microscopy

WHO world health organization

List of Tables

List of Figures

List of Equations

To Louka and Félix

The roots of education are bitter,
but the fruit is sweet

Aristotle

Acknowledgements

This work could not have been accomplished without the help and guidance of my research director Dr. Caroline Duchaine. During the past five years of working in her laboratory, Dr. Duchaine gave me the opportunity of working on various projects allowing me to acquire different skills in scientific research and even more in being an effective group member. Comparable to a mother teaching her child, she knew when and how to encourage, reassure and restrain me. I consider myself a lucky man to have been part of her team and I sincerely hope that someday our paths will cross again to initiate other hazardous and peculiar projects.

I would like to thank my good friends Dr. Francois McNicoll, Dr. Christian Laflamme and Dr. Daniel Verreault for introducing me to Caroline's laboratory and for initiating my training in scientific research. I would also like to thank all present and past members of the team that contributed in anyway to my growth as a young scientist and supported me during my early scientific development: Dr. Steve Dutil, Dr. Yan Gilbert, Marc Veillette, Dr. Valérie Létourneau, Dr. Nathalie Turgeon, Geneviève Filion, Pascale Blais-Lecours, Hubert Morissette-Rouleau, Marie-Josée Toulouse, Mélissa Marcoux-Voiselle, Rémi Charlebois, Martyne Audet, Dr. Phillipa Perrott, Dr. Laetitia Bonifait, Éric Jubinville and Léa Gauthier-Lévesque.

I offer my most sincere acknowledgments to Anne Mériaux for her relentless work in order to obtain the proper certifications and permits required for the bacterial strains needed.

I am thankful to Dr. Daniel Côté for accepting the task of being my co-director and for providing insightful training during examinations and classes, to Olivier Dupont for his time spent on coding the MatLab program for this project and to Christian Tardif for providing part of the code, to David Emond for statistical analysis, to Dr. Sylvain Moineau and his team for accepting me in their meetings and providing useful information on the bacteriophage models and the associated laboratory methods, to Dr. Simon Rainville who, at the last minute, accepted to be part of my advisory committee and offered a different perspective to this project.

I am grateful to Dr. Paul De Koninck for accepting me in the Biophotonics program, to Dr. Mario Méthot who, as the main program coordinator, helped me at numerous occasions during my training. I would like to thank the Natural Sciences and Engineering Research Council of Canada (NSERC) who, through The Collaborative Research and Training Experience (CREATE) Program, financially supported my training during this project.

I am also thankful to Dr. Denis Boudreau and his students: Danny Brouard and Félix-Antoine Lavoie, who provided support and equipment for the spectroscopy and fluorescence-lifetime imaging microscopy analysis.

I am forever indebted to professor Yasunori Tanji and his team for providing the GFP expressing PP01 bacteriophage, and to Philippe Thomen and his team for providing the lysogen

strain containing λeyfp bacteriophage. Without their provision, this project would not have been possible.

Finally, I would like to thank my family. My parents, Mark and Shirley, who always supported me in my multiple endeavors hoping that someday, their son would find a suitable path that would lead to stability and happiness, I do believe that it has happened. My love, with whom I face my various challenges and that, together, we experience an indescribable life of blessedness with our children, Louka and Félix.

I assume that I am forgetting some people, and if so, they will know that I am greatly appreciative of their support and help received throughout the years. Thank you all.

Preface

The presence of airborne viruses in the environment constitutes a menace for human health and social economy. To fully understand the impact of airborne viruses on our society a new field of study came into existence: aerovirology. At the time of this writing, aerovirology is arising as a new transdisciplinary science integrating academic researchers and medical practitioners from different unrelated backgrounds, such as theoretical physicists, engineers, virologists and health care professionals. The methods and tools developed by such a heterogeneous team are indispensable in order to better explain the complexity of viroaerosol transmission. Computer simulations produce interesting theoretical data on aerosol concentration and distribution in various settings, *in vitro* aerosol chamber studies provide essential information on air sampling techniques and environmental factors affecting the recovery of airborne viruses, and field research helps elucidate the role of airborne viral transmission in real world conditions. Aerosol science explains the principles behind airborne sampling and aerosol behavior, however, it ignores the physical attributes of biological entities that substantially modify the way of collecting and analyzing airborne particles. Therefore, tools used for sampling inorganic compounds may not be suitable for recovering viroaerosols that are more often propagated with biological material. Furthermore, detecting viruses in airborne samples requires distinct virological methods according to the molecular biology and infectivity potential of the viruses. The integrity of a virus will ultimately depend on how and with what it was aerosolized, the environment in which it was found and how it was collected. Then, one may evaluate the potential that a given airborne virus could infect its host. Altogether, aerovirology aims at answering questions related to the possible transmission of viruses through the airborne route. To adequately do so, new tools must be designed and brought forth to expand our knowledge on this subject. This manuscript will present the use of new models and cutting-edge techniques in order to study viroaerosols and propose a new approach to investigate this subject.

Chapter 1

Introduction

1.1 General introduction

Airborne transmission of potential lethal viruses is attracting global concern since researchers demonstrated that a possible human pandemic influenza virus could acquire this ability under natural conditions [29]. Moreover, the world health organization (WHO) and other partners are currently investigating a new strain of coronavirus associated with severe respiratory disease that could spread through the air [18]. The mechanisms responsible for this route of transmission are still poorly understood, thus, research related to viroaerosol characteristics is critical in order to improve and choose the right approach to handle airborne viral outbreaks. Previous studies have described to a certain extent the importance of multiple factors affecting the stability and transmission of airborne viruses, such as, **relative humidity** [1, 5, 6, 12, 13, 24, 30, 33, 35, 39, 41, 43, 56, 60, 61, 62, 64, 66, 67, 73, 74], **temperature** [28, 30, 33, 34, 39, 41, 43, 62, 74], **radiations** [13, 19, 47, 48, 49, 72], **medium** [4, 3, 6, 24, 23, 25, 33, 34, 40, 61], and also the **concentration** and **size distribution** of the aerosol [42].

These characteristics will also determine how the viroaerosol will penetrate and deposit in the different regions of the respiratory system. However, the key property for characterizing respiratory deposition, and the efficiency of different types of air purifying units, is the aerodynamic diameter of particles in aerosols. This is defined, for a given particle, as the diameter of the spherical particle with a density of a water droplet (1 g per cm^3) that has the same settling velocity as the particle [31]. If a particle has an aerodynamic diameter of 1 μm, it behaves like a 1 μm spherical water droplet no mater its shape, density, or geometric size. Many instruments such as cascade impactors and time-of-flight apparatuses (figure 1.1) use aerodynamic properties to determine aerodynamic particle size distribution. Time-of-flight technique is used to measure the aerodynamic diameter of particles and to determine their airborne and deposition behavior. For humans, particles in the 3 μm size range are capable of circulating more easily through the pulmonary airways down to the alveolar region of the

lungs and ultimately cause infection and disease [31]. However, deposition of particles is highly variable and depends on several factors, including flow rates, type of breathing used, and particle size. Increased knowledge of virus aggregation in aerosol particles together with their aerodynamic properties is essential to better monitor, detect and prevent viral transmission. Consequently, experiments using controlled conditions are required to assess the given factors affecting these characteristics.

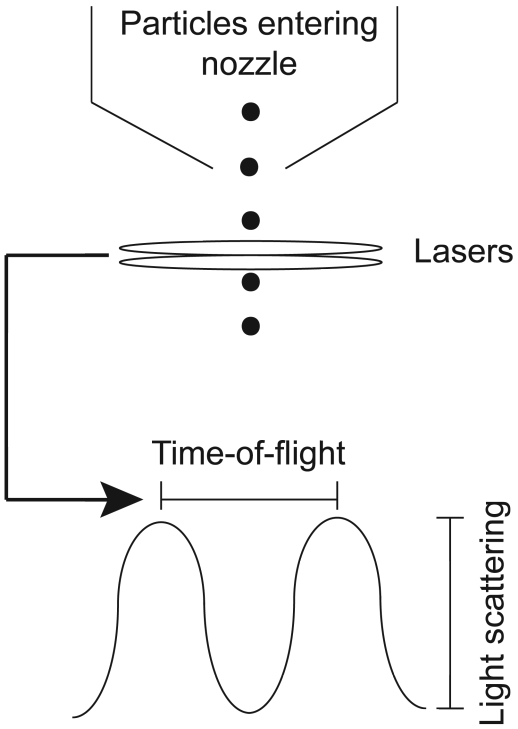

Figure 1.1: Particles are accelerated through a nozzle at high velocities. At the nozzle exit, particles pass through two laser beams, one by one. The time-of-flight between the two laser beams is measured for each particle and by using an specific algorithm, an aerodynamic size can be given to each particle.

1.2 Aerosols, bioaerosols and viroaerosols

An aerosol can be define in a rather simplistic way as a suspension of solid or liquid particles in a gas [31]. However, aerosols can be categorized subsequently into more complex classes according to the physical properties of their particles and their origins: biological or inorganic, natural or anthropogenic, monodisperse or polydisperse. A solid-particle aerosol can be referred to as either dust or fume. The former forms during mechanical disruption of a parent material (crushing or pulverizing) and usually generates particles greater than 0.5 μm in diameter. The latter is generally produced after combustion of solid substances and is composed of particles smaller than 1 micron. Fog, a liquid-particle aerosol, is formed by

the condensation of vapors resulting in spherical particle ranging from 0.1 μm to about 200 μm in size (ex. oil fog associated to metalworking fluids in a factory). Spray is another form of aerosol constituted of liquid particles. Larger than a few microns, it is obtained after the atomization or nebulization of a liquid (ex. the nebulizate created by a medical inhalator) [21]. Liquid aerosols contain droplets that, if small enough ($<$ 10 μm), dry up quickly and form what is called a droplet nuclei (figure 1.2), and when formed, a droplet nuclei becomes a dried solid- particle aerosol following the same laws of physics.

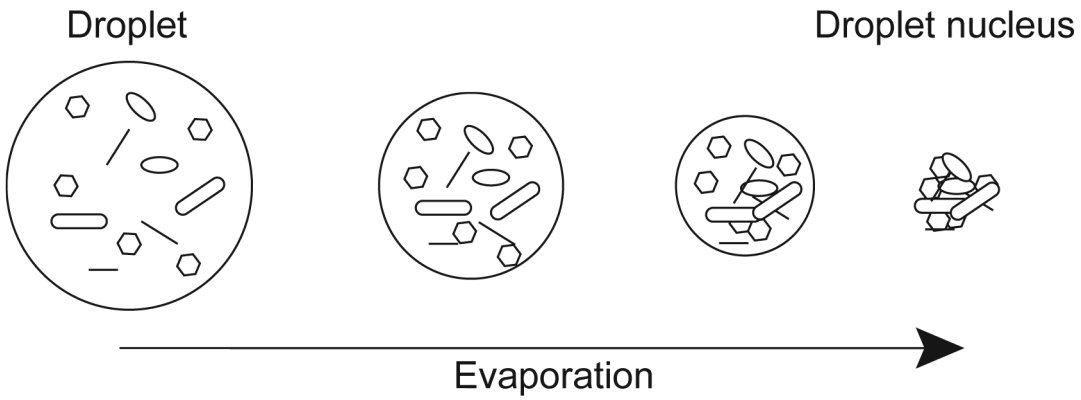

Figure 1.2: Evaporation of a liquid droplet to a droplet nucleus. As the liquid evaporates, the non-evaporative content concentrates until a droplet nucleus is obtained.

Smoke is a visible aerosol obtained after the incomplete combustion of a liquid or solid material. Investigators have reported a size range of 0.3 to 0.5 μm in diameter [9] with the presence of ultrafine particles ($<$100 nm) but particles can agglomerate to form larger compounds (ex. cigarette smoke). Smog is the visible pollution of the atmosphere. The term comes from the contraction of the words smoke and fog [20] and it is the result of the condensation of water (fog) on particles in suspension (smoke) with the presence of ozone (O_3) from the troposphere. Smog has many different adverse effects on human health. It is associated to irritations of the eyes, nose and throat, to breathing difficulties, to the aggravation of symptoms related to respiratory diseases, to cardiac problems, and to premature deaths [21]. Aerosols can originate from natural, human or industrial activities and are formed by different mechanisms such as nebulization, attrition, re-suspension, condensation, etc. Natural aerosols include aerosols generated by wind, waves, tornadoes, volcanoes, climatic condensation, etc. Coughing, sneezing, talking, walking and cleaning are examples of aerosols produced by human activities. Among the industrial activities creating aerosols, there is the action of turf bagging, waste-water treatment plants, garbage collection, animal farming, etc [21]. The residence time of particles in the air will mainly depend on the properties and origins described above. Greater sized particles ($>$200 μm) will travel only a couple of meters before reaching the ground or a surface compared to droplet nuclei that can stay airborne for hours before settling or getting inhaled (figure 1.3).

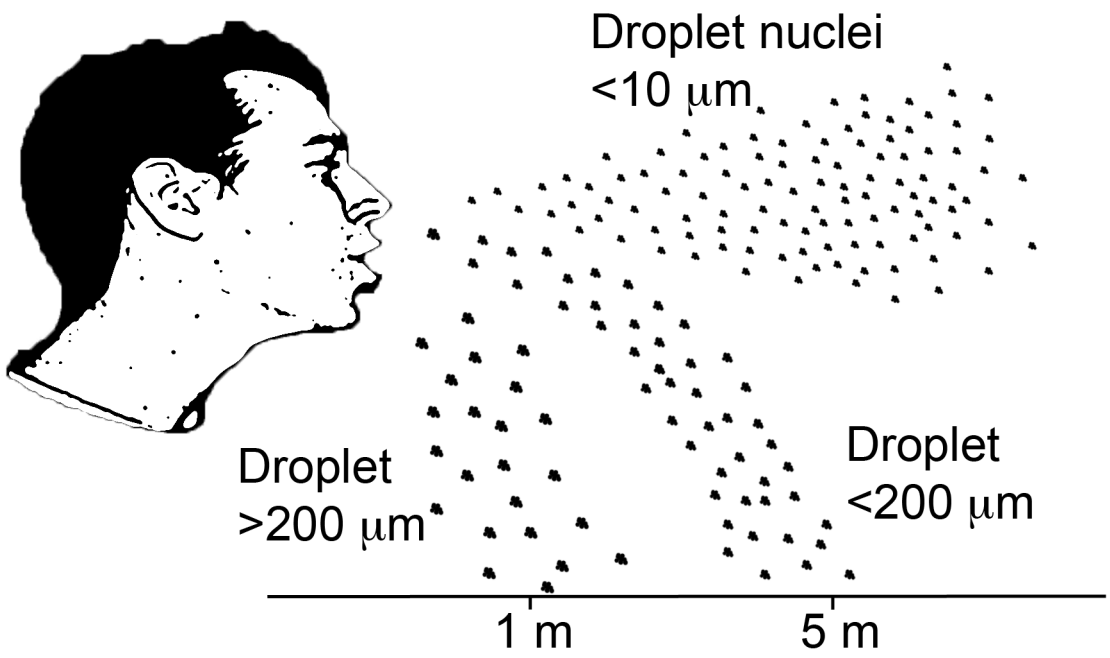

Figure 1.3: The distance of flight associated to the size of airborne particles.

Bioaerosols are aerosols constituted of living microorganisms or molecules originating from biological entities (viruses, bacteria, fungi, algae, fragments of plant or animal cells, toxins, proteins, nucleic acids, etc.). Their size can vary from a couple of nanometers to hundreds of micrometers. A major distinction between aerosols and bioaerosols is that the latter has the capacity of infecting a suitable host, replicate and then reenter the airborne state. A suitable host can either be a human, an animal, a plant or even a product that, when exposed to a given biological agent, would acquire undesirable effects. Some major infectious diseases are transmitted as bioaerosols and can be classified on the basis of their infectivity when airborne as either obligate, preferential, or opportunistic airborne transmitted pathogens [10]. Obligate airborne transmitted diseases occur only by deposition of droplet nuclei containing pathogens in the distal lung under natural conditions. This is the case of tuberculosis, a sickness caused by the bacterium *Mycobacterium tuberculosis*. Preferential airborne transmission refers to pathogens, such as the Morbillivirus (Measles) and Varicella zoster virus (chickenpox) [57], that can initiate infection by multiple routes, but are predominantly transmitted by droplet nuclei. Finally, diseases that are usually contracted by other routes (droplets, direct physical contact or faecal-oral) but that can also initiate infection through the distal lung are referred to as opportunist airborne transmitted pathogens. The severe acute respiratory syndrome (SARS) coronavirus and influenza viruses are part of this group. Probably many diseases are opportunistically airborne transmitted, however, the lack of knowledge on bioaerosol transmission limits our view at the moment. The viability or infectivity of an airborne microorganism is directly related to environmental factors, such as: temperature, relative humidity (RH), pH,

UV rays, the nature of the microorganism and with what it is co-aerosolized [21].

Viroaerosols are aerosols containing viruses or viral molecules. Since they are extremely small, biologically speaking, and are obligate parasites (they cannot complete their life cycle without using a suitable host), viruses are easily aerosolized and propagated through droplet nuclei.

1.3 Methods for sampling viroaerosols

A recent review by Verreault *et al.* [70] describes in detail the different methods for sampling airborne viruses. The most well-known samplers include solid and liquid impactors, filters, cyclone samplers, liquid impingers, slit samplers and electrostatic precipitators, and filters. Solid impactors, such as the one used in this study: the Andersen six-stage impactor, collect particles according to their size distribution in which each stage traps particles of a specific aerodynamic diameter size range. At a 28.3 L/min flow rate, the measured d_{50} of particles trapped from stage one to six of the Andersen six-stage impactor are 7 μm, 4.7 μm, 3.3 μm, 2.1 μm, 1.1 μm and 0.65 μm, respectively [76]. Also, the different stages can correspond to different human lung deposition sites (figure 1.4).

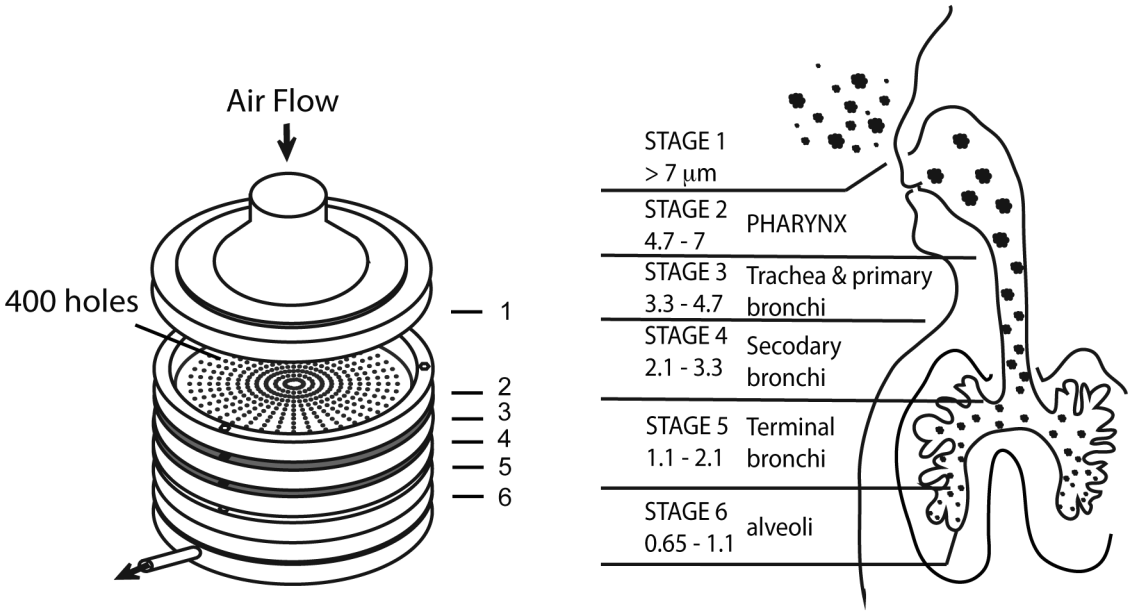

Figure 1.4: The Andersen six-stage impactor.

1.4 Methods for analyzing viroaerosols

The analytical procedures used are also crucial elements to consider for providing accurate information about the condition and quantities of viroaerosols. The most common methods are cell culture methods, such as, plaque assay (figure 1.5) to determine the infectious load of

viroaerosols and molecular biology techniques, such as, SYBR Green quantitative polymerase chain reaction (qPCR) (figure 1.6) for genome quantification. Plaque assay can be performed by preparing 10-fold dilutions of a virus stock, and 0.1 ml aliquots are deposited onto a susceptible cell lawn grown on a culture medium. After the proper incubation period, infectious particles produce circular zones of infected cells called plaques, and eventually become large enough to be visible to the naked eye and then, be counted to determine the infectious load of a sample. One plaque is produced by one infectious particle and only the viruses that are infectious can be assayed in this way. For SYBR Green qPCR, an initial amount of nucleic acid in a sample can be quantified by amplifying a specific region of a gene or genome using the double-stranded (dsDNA)-binding SYBR Green I dye and proper reagents and instrumentation for real-time detection. The dye's fluorescence signal increases in proportion to the amount of double-stranded deoxyribonucleic acid (dsDNA) generated during the amplification steps. With a calibration curve produced by using a known amount of the specific gene segment of interest, virus genomes can be precisely quantified in samples. These two analytical procedures are widely used in aerovirology and can offer a good overall view of a viroaerosol sample, however, while these techniques are becoming indispensable, they lack the ability to analyze viroaerosols at the particle level.

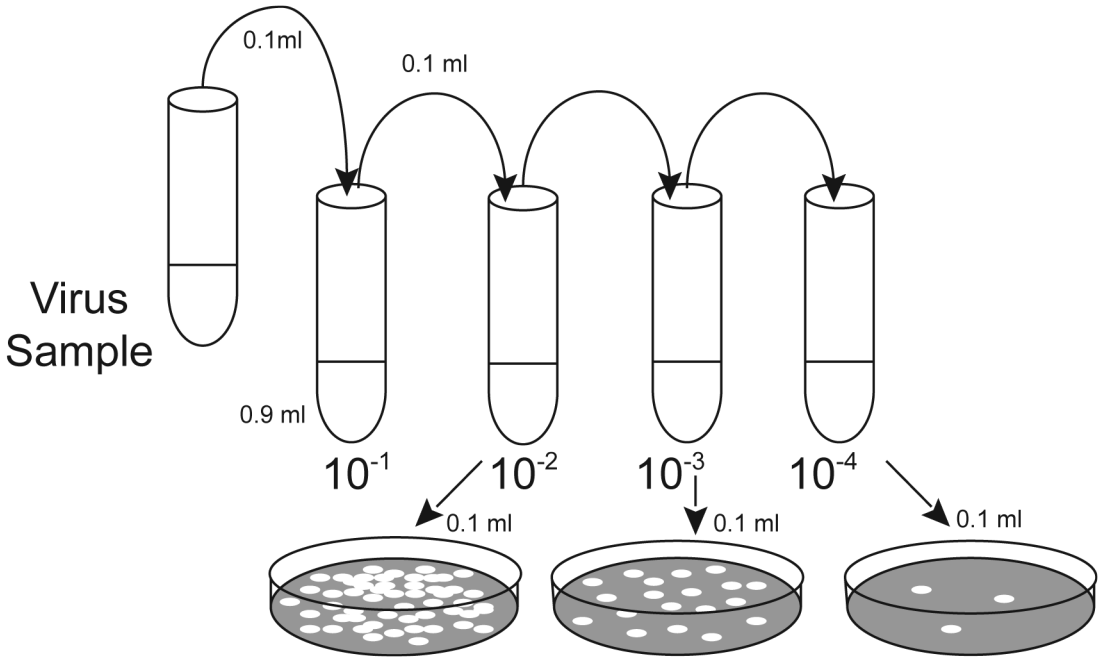

Figure 1.5: The plaque assay method.

Standard epi-fluorescence microscopy (EFM) is frequently employed in cell biology studies to reveal information regarding cellular morphology, intracellular ion concentrations, protein binding, lipid content, and membrane permeability [58]. It has also been used, coupled with the proper fluorescent molecules, in microbiology to enumerate bacteria and viruses in liquid

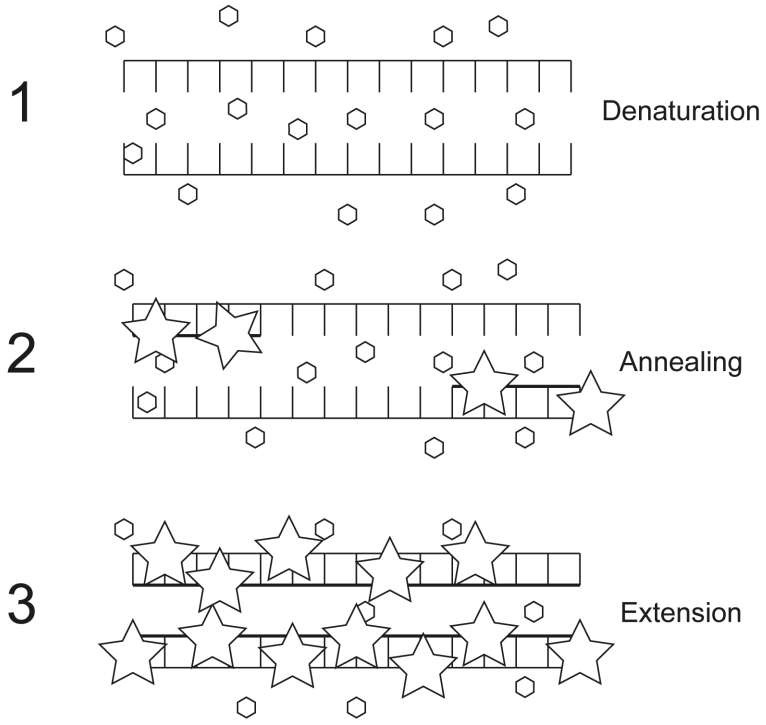

Figure 1.6: The SYBR Green qPCR method: (1) during the denaturation step, dsDNA is separated at high temperature to allow (2) the specific primers to anneal to the regions of interest on the single-stranded DNA. (3) A DNA polymerase then extends the primers to synthesize complementary dsDNA amplicons were the SYBR Green I can bind and produce fluorescence signals. Fluorescence signals are analyzed every amplification cycle and can be compared to a standard curve for proper quantification.

samples [63], and in some cases it was found to be more accurate than traditional cell culture methods [53]. Imaging and quantification of virus fluorescence signals has been developed to be used on aquatic aggregates in order to gather information on viral spatial distribution and was proposed as the method of choice for these types of investigations [44]. To our knowledge, this method of viroaerosol analysis has never been used in aerovirology. EFM combined to appropriate virus models could offer new insights on viral aggregation in aerosols and information on the virus load per aerosol particle. However, standard fluorescence microscopy has also its limitations: intensity variations of the excitation source, optical loss in the optical path or sample, variation in sample fluorophore concentration, photo-bleaching, and microscope centering [16]. Moreover, fluorophores with similar excitation and emission spectra may be impossible to differentiate with this type of analysis.

For this reason, fluorescence-lifetime imaging microscopy (FLIM) would be a good option to counter some of these disadvantages. FLIM produces images of the fluorophore's lifetime (the property describing how rapidly fluorescence decays), providing another dimension of information for visualizing fluorophores and an additional source of contrast. As an example,

while having very similar excitation and emission spectra, green fluorescent protein (GFP) can be distinguished from Fluorescein isothiocyanate (FITC) molecules in lifetime imaging regardless of the fact that their spectra overlap [36]. Using FLIM technology would increase the sensitivity of detecting and quantifying fluorescent signals by removing unwanted background contaminating aerosol samples and in addition, it could offer the possibility of analyzing single particle viroaerosols.

The various analysis methods also have different purposes, advantages and limitations (Table 1.1). Consequently, the use of one technique will neglect the information provided by the others. For example, fluorescence microscopy can provide data on the number of viral particles in a sample, however, information on the infectivity and molecular biology of the virus would be missing. On the other hand, fluorescence microscopy can be done with samples collected on a solid medium while the other methods cannot. Therefore, a fundamental component indispensable to aerovirology investigations is an appropriate laboratory model. The choice of a good airborne virus model should be based on its versatility to cope with the different collection and detection methods utilized and, furthermore, its similarities with the viruses intended to simulate. For these reasons, bacteriophages are interesting models for aerovirology research.

Table 1.1: Characteristics of the selected analysis methods.

Technique	Assessment	Sample type	Reproducibility	Time	Cost
Plaque assay	Infectivity	Liquid	Poor	Days	Low
qPCR	Genome	Liquid	Excellent	Hours	High
Fluorescence microscopy	Viral particle	Liquid / Solid	Good	Hours	Moderate

1.5 Bacteriophages as airborne virus models

Bacteriophages (a.k.a. phages) are viruses that infect and replicate within bacteria. Compared to animal viruses, they have structural differences, such as, protein tails that attach to the bacterial cells in order to inject their genomes for replication. They are considered the most abundant and ubiquitous organisms in the biosphere [17]. In laboratory, they are relatively easy to propagate, safe to manipulate and no particular handling or specialized facilities are required. In addition, genetically modified fluorescent phages already exist to facilitate research involving visualization and quantification using fluorescence microscopy systems. As shown in table 1.2, fluorescent phages are ideal in order to explore the different aspects of viroaerosols (infectivity potential, genome, particle distribution). In this study, two genetically modified phage models and one phage stained with a DNA-binding fluorophore were used and also compared to a non-biological fluorescent microsphere model. The models are

briefly presented in figure 1.7 and the fluorescence spectra of their fluorescent molecules are presented in figure 1.8.

Table 1.2: Analysis methods vs virus models.

Model	Plaque assay	qPCR	EFM
Phage	+	+	- (+)*
Phage expressing FP	+	+	+
Fluorescent microsphere	-	-	+

* While stained with fluorescent dye

FP: Fluorescent protein

The first model is phage PP01-SOC/GFP, a tailed, double-stranded DNA (dsDNA) recombinant phage of the *Myoviridae* family engineered to display green fluorescent proteins (GFP) on the small outer capsid (SOC) of the virion. This phage was previously used to detect *Escherichia coli* O157:H7 strains in water samples [50]. As many as 960 SOC molecules decorate the head of T-even phages [37] and each molecule exposes a GFP. The second phage model is λeyfp, a genetically engineered λ phage of the *Siphoviridae* family that carries a capsid protein gpD fused to the enhanced yellow fluorescent protein (EYFP). This model was created to provide information on the propagation of fluorescent viruses in growing plaques [7]. The third phage model was wild-type P008, another tailed, dsDNA virus of the *Siphoviridae* family with a 53 nm in diameter isomeric capsid that was previously used in aerovirology experimentation [71]. This phage model was stained prior to analysis with the dsDNA-binding dye: SYBR Gold. The last model is the non-biological 50 nm YG microsphere that have been frequently used in phagocytosis studies, flow cytometry and diagnostic assays. Some of the fluorescence characteristics of the phage models are presented in table 1.3. The molar molar absorption coefficient (ϵ) is basically the strength of a molecule for absorbing photons at a given wavelength and is dependent on the concentration and light path-length of a given specie in a sample. The quantum yield quantum yield (η) is the fraction of photons re-emitted as fluorescence after absorption. Finally, the brightness of a fluorophore is obtained by dividing the product of the (ϵ) and the (η) by 1000, and usually is a good indicator for choosing an adequate fluorophore.

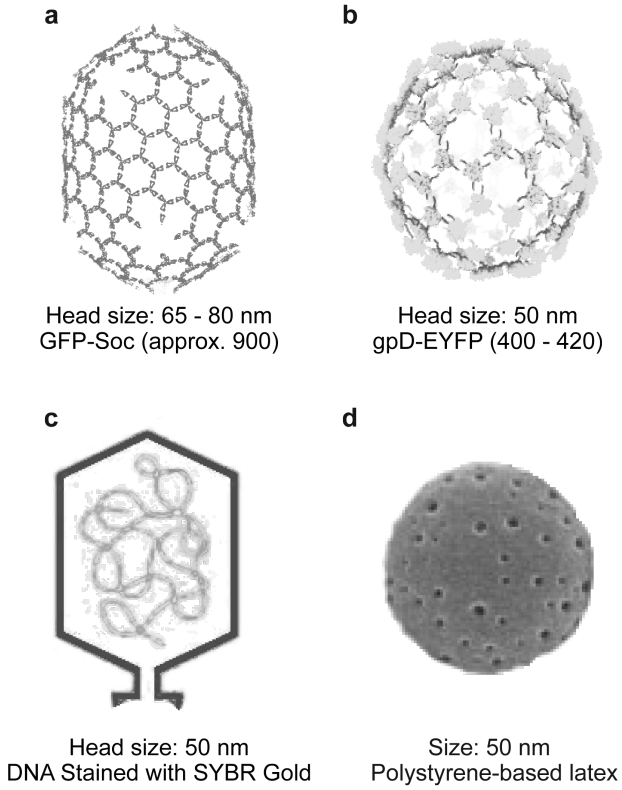

Figure 1.7: Images of the four virus models used in this study: (a) displays a cryo-electron micrograph of wild-type phage T4 Soc-cage (adapted from Qin et al [55]) representing the chimeric GFP/Soc proteins of the PP01-GFP model (approx. 900 per virus), (b) shows a modified image of a lambda phage gpD-cage (adapted from Lander et al [38]) representing the chimeric EYFP/gpD proteins of the λeyfp model (approx. 410 per head), (c) portrays the head of the P008 model showing the packaged DNA stained with the SYBR Gold fluorophore, and (d) is a scanning electron micrograph of a polystyrene-based latex particle representing the YG microsphere model (adapted from Tong and Deng [65]).

Table 1.3: Characteristics of the selected virus models.

Model	Ex/Em max (nm)	ϵ ($M^{-1}cm^{-1}$)	η (%)	Brightness
YG microspheres (FITC)	441/486[a]	78534	99	77.75
λeyfp	513/527[b]	83400	61	50.87
PP01-GFP/SOC (EGFP)	496/512[c]	55000	60	33
P008-SYBR Gold	495/537[d]	>50000	>90	>45

[a] Fluoresbrite Microspheres (2009). Polysciences, Inc. Rev. #005, Technical Data Sheet 431

[b] 2002, Becton, Dickinson and Company

[c] Kimata *et al.* (1997). A Novel Mutation Which Enhances the Fluorescence of Green Fluorescent Protein at High Temperatures. Biochemical and Biophysical Research Communications 232:69-73

[d] SYBR Gold Nucleic Acid Gel Stain (2006). Molecular Probes Inc. Manual MP 11494

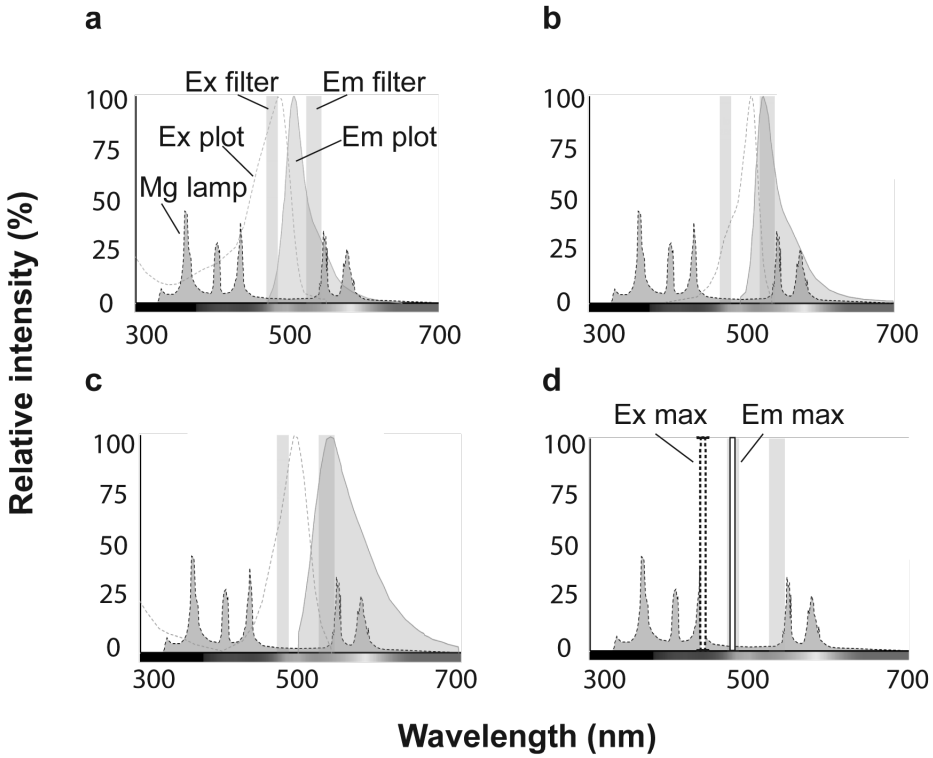

Figure 1.8: The fluorescence spectra for the four different virus models with the Ex and Em bandwidths of the FITC Filter cube, and the Ex plot for the mercury (Mg) lamp of the epi-fluorescence microscope used in this study: (a) λeyfp, (b) PP01-GFP model, (c) P008-SYBR Gold, and (d) YG microspheres (no spectra has been found).

1.6 Problematic

As mentioned previously, to our knowledge, no virus model nor analysis method offers the possibility to analyze viroaerosols at the particle level. Specific information about single viroaerosol particles is unexplored, therefore, distribution of viruses in relation to the size of aerosol particles is unknown. More knowledge on the precise distribution of viruses in aerosols would provide helpful insights on how to better control and eliminate unwanted viroaerosols in different settings.

1.7 Hypothesis and aims of this study

The hypothesis of this study is that the fluorescent bacteriophage models will behave the same way as non-fluorescent models for aerosolization, collection and analysis (plaque assay and qPCR). Furthermore, the use of fluorescence microscopy analysis on air samples from the fluorescent models will provide accurate information on the quantities, distribution and sizes of the viroaerosols in the laboratory settings.

The aim of this study was to evaluate the feasibility of using a fluorescent bacteriophage coupled to EFM as a new method to study viroaerosols characteristics. First, the overall infectivity, genome copy number, viral particle number and size distribution of the fluorescent expressing PP01-GFP/SOC, λeyfp and non-fluorescent P008 viroaerosols were compared. Afterward, single-particle analysis of fluorescent viroaerosols using EFM, FLIM and virus model λeyfp was conducted to quantify viral load on solid medium.

Chapter 2

Materials and Methods

2.1 Viral models

Bacteriophage P008 and its bacterial host, *Lactococcus lactis* F7/2A, were obtained from the Felix d'Hérelle Reference Center for Bacterial Viruses (http://www.phage.ulaval.ca/). Fluorescent bacteriophage PP01-GFP/SOC was provided by professor Yasunori Tanji's laboratory (Department of Bioengineering, Graduate School of Bioscience and Biotechnology, Tokyo Institute of Technology, 4259 J2-15 Nagatsuta-cho, Midori-ku, Yokohama 226-8501, Japan) and *Escherichia coli* O157:H7 (CIP 105917) obtained from the Collection de l'Institut Pasteur (25-28 rue du Docteur Roux, 75015 Paris, France) was used as the bacterial host. Fluorescent bacteriophage λeyfp was provided with its host, *E. coli* NM538 by the Laboratoire Pierre Aigrain (École Normale Supérieure-Université Pierre et Marie Curie, 24 rue Lhomond, 75005 Paris, France). Fresh stocks of P008 and PP01-GFP/SOC bacteriophages were prepared by small-scale liquid cultures. Phages were propagated under agitation in flasks containing proper bacterial host and culture media: M17 Broth supplemented with 0.5% glucose and 10 mM of $CaCl_2$ for phage P008 and Tryptic Soy Broth (Becton, Dickinson and Company, Sparks, MD, USA) for PP01-GFP/SOC. Cultures were incubated either at 30°C for P008 or 37°C for PP01-GFP/SOC. Phages were added when the bacterial culture's OD600 reached approx. 0.1 and incubation was carried on for 2 to 3 h until cells had lysed. Bacteria containing the prophage of λeyfp were incubated O/N at 30°C, then, a heat shock treatment at 45°C for approx. 15 min was done to activate the lytic cycle of the phage. Incubation was carried on at 37°C for 2 hours or until bacterial lysis occurred. Bacteria and debris were removed by centrifugation at 4000 X g for 10 min at room temperature. The phage-containing supernatants were filtered (0.45 μm) and then kept at 4°C. Phage amplifications produced approximately 10^{10} plaque forming unit (PFU) per ml as determined by plaque assay [2]. Fluoresbrite 0.05 μm YG microspheres (Polysciences Inc., Warrington, PA, USA) were also used to compare aerosolization and fluorescence properties to the fluorescent bacteriophages. A 100-fold dilution in distilled water of the main stock solution was used for all experimentation in this study

to obtain comparable concentrations with phages in analysis.

2.2 Generation and monitoring of viroaerosols

Aerosolization was performed in a 3.36 liter GenaMINI chamber (SCL Medtech Inc., Montreal, QC, Canada). The experimental design has been previously used for the aerosolization of DNA phages [71], ribonucleic acid (RNA) phages [27] and the Newcastle disease virus [68]. Specifications for the aerosolization setup are detailed elsewhere [71] and figure 2.1 displays the fundamentals of the setup. One mL of a virus lysate was mixed with 69 ml of phage buffer (Tris-HCl 10 mM, pH 7.4, NaCl 100 mM, MgSO4 10 mM) into a nebulizer (Single-Jet Atomizer, model 9302, TSI Inc., Shoreview, MN, USA) that generated aerosols at a rate of 3 L/min using HEPA-filtered medical air. Aerosols passed through a desiccator (model 3062, TSI Inc.) containing the desiccant blue beads (EMD Chemicals Inc., Gibbstown, NJ, USA; Cat. # EM-DX0017-3) allowing the formation of droplet nuclei before entering the chamber. While entering the chamber, the aerosol was diluted with HEPA-filtered medical air at a rate of 30 L/min.

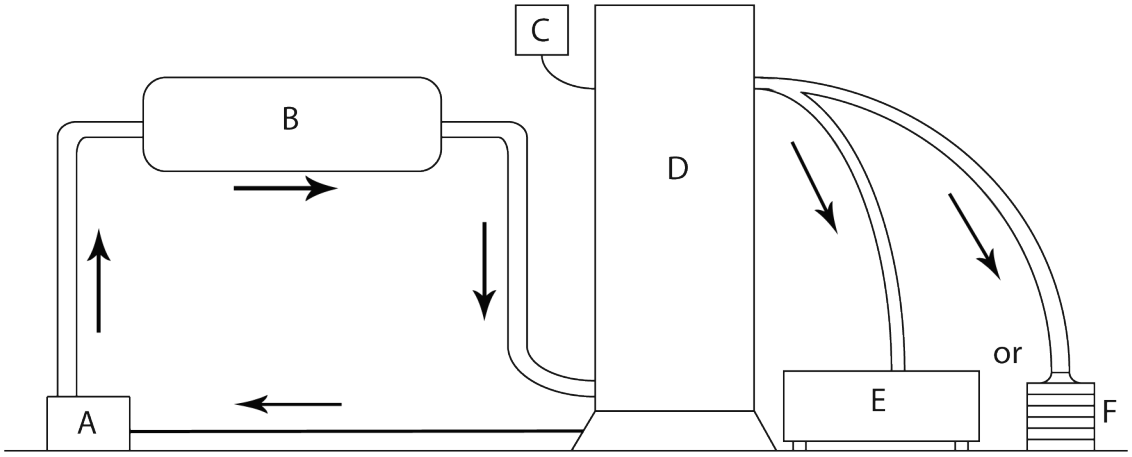

Figure 2.1: An airflow is generated from the chamber (D) to the nebulizer (A) containing the virus model in the liquid medium. Aerosols are generated at 3 L/min and flow through the desiccator (B) before penetrating into the chamber. Aerosols are either analyzed with the aerodynamic particle sizer (E) or collected using the six-stage Andersen impactor (F). During experimentation, the thermo-hygrometry probe measures the temperature and relative humidity inside the chamber (C).

An aerosol particle sizer (APS) (model 3321, TSI Inc.) spectrometer connected to an Aerosol diluter (model 3302A, TSI Inc.) was used to monitor particle size distribution and concentration inside the chamber. Data was collected every minute for a period of 10 min before and after each aerosol sampling.

A Kistock datalogger KH-210-DO (Kimo instruments, Montpon, Dordogne, France) was also

connected using its external thermo-hygrometry probe to measure the temperature and relative humidity (RH) inside the chamber.

2.3 Collection and recovery of viroaerosols in liquid media

Air samples were collected using a six-stage Andersen impactor (Andersen Instruments Inc., Atlanta, GA, USA) [8] loaded with Petri dishes containing 20 ml of phage buffer. The sampling time when using the Andersen impactor was of 10 min at 28.3 L/min for a total of 283 L of aerosol collected. The impactor was connected to a Gilair Aircon II pump (Levitt Sécurité, Montreal, QC, Canada) and the flow rate was calibrated to 28.3 L/min with a DryCal DC-2 primary flow calibrator (Bios International Corporation, Butler, NJ, USA).

2.4 Analysis of viroaerosols in liquid media

Aerosol samples were quantified using three different methods: quantitative polymerase chain reactions (qPCR) for the genome copy numbers, plaque assays for the infectious load and EFM to visualize and enumerate viral particles.

2.4.1 qPCR

All qPCR reactions were performed with the DNA Engine Opticon 2 Real-Time PCR Detection System (Bio-Rad Laboratories). Samples were analyzed using the Opticon Monitor Software version 2.02.24. The primers used for detecting and quantifying P008 genomes were designed and used in a previous study [71]. For λeyfp, primers used in another study [22] for detection improvement were chosen. For PP01-GFP/SOC, primers were designed using invitrogen's OligoPerfect Designer (www.invitrogen.com). Forward primer PP01-GFP/SOC F (5'- GTC CAC ACA ATC TGC CCT TT-3') targeted the *gfp* inserted between *soc1* and *soc* genes, and the reverse primer PP01-GFP/SOC R (5'-TCT GAT AAT GAG CGC CAG AA-3') targeted the *soc* gene. The amplified region corresponded to a DNA fragment of 229 bp. The qPCR reaction mix contained 1X final concentration of iQ SYBR Green Supermix (Bio-Rad Laboratories), 0.5 μM of forward and 0.5 μM of reverse primers and 5 μl of the desired test sample. The qPCR samples were adjusted to a final volume of 25 μl with sterile water. The amplification cycle was: 94°C for 3 min followed by 35 cycles of 94°C for 20 sec, 60°C for 30 sec, plate read and 72°C for 25 sec. A melting curve from 50°C to 95°C was done at the end to establish that the right amplicon was obtained. All qPCR assays were performed in triplicates. Plasmid standards were constructed to quantify the viral genome copy numbers. Briefly, qPCR was performed on the phage lysate with the same specific primers and conditions as described above. The desired amplicon was purified using the QIAquick PCR purification kit (Qiagen Canada Inc., Mississauga, ON, Canada) and cloned into the pCR4-TOPO vector following the protocol in the TOPO TA Cloning kit (Invitrogen Inc.,

Burlington, ON, Canada). Transformation was done into Invitrogen's chemically competent *E. coli* TOP10 cells and plasmid DNA was purified using Qiagen's QIAprep Spin Miniprep Kit. Serial dilutions from the resulting clones were used as standard curves for qPCR assays, each containing a known amount of input copy number.

2.4.2 Epi-fluorescence microscopy

Sample preparation

For fluorescent particle visualization and enumeration, samples were prepared following a modified version of a protocol described elsewhere [52]. Ten-fold serial dilutions of the test samples were done in phage buffer in order to obtain between 10 and 1000 fluorescent particles per microscopic field. For P008, SYBR Gold Nucleic Acid Gel Stain (Invitrogen Inc.) was added at a final concentration of 1X and incubated in the dark for 10 min at room temperature. Afterwards, dilutions were filtered onto 0.025 μm MF-Millipore membranes (Millipore Corporation, Billerica, MA, USA) to capture viral particles. Filters were then mounted onto microscope slides with a drop of antifade solution (MOWIOL 4-88 Reagent; EMD Chemicals Inc., Gibbstown, NJ, USA) between the filter and the coverslip. All preparations were performed in a room with the least amount of light possible to ensure proper care of the samples.

Image acquisition and analysis

Pictures were taken with a QImaging Retiga 1300 digital CCD camera (QImaging, Surrey, BC, Canada) connected to a Nikon E600 Upright Epi-Fluorescence Microscope System (Nikon Instruments Inc., Melville, NY, USA) in 10 randomly selected fields at 100X magnification using the FITC spectral filter (Excitation: 480/30, Emission: 535/40). The software Simple PCI version 5.1 (Campix Inc., Cranberry Town, PA, USA) was used for image acquisition and MATLAB R2010b (MathWorks Inc., Natick, MA, USA) was used for image processing and analysis. The code and its usage is detailed in Annexe A. The total fluorescence intensity signals and area size per particle in the nebulization media images were used to determine the fluorescence characteristics for single viruses. The fluorescence data gathered from particles from images of the Andersen stages samples was then divided by the values obtained for single viruses resulting in the number of viruses per particle. The sum of virus particles per image was then multiplied by the ratio (22140.05) between the area size on the filter (130.3 mm^2) and the image's area size (5883.8 μm^2) resulting in the number of viruses per ml of sample. Finally, for air samples, the number of viruses per ml was multiplied by the quantity of liquid on the stage of the Andersen sampler (20 ml) and divided by the total amount of air collected by the sampler (283 L of air) resulting in the number of virus particles per L of air.

2.4.3 Fluorescence spectroscopy

Fluorescence spectroscopy assays were performed using a Synergy H1 Hybrid Multi-Mode Microplate Reader (BioTek Instruments Inc., Winooski, VT, USA) and measurements were taking using the green filter set (Excitation: 485/20, Emission: 528/20). Samples were analyzed using BioTek's Gen5 Data Analysis Software, in triplicates and were subjected to blank subtractions. A standard was generated for each model by using the fluorescence intensity data from ten-fold dilutions of the nebulization medium. Each dilution was analyzed in EFM to determine the quantity of fluorescent particles related to the given fluorescence intensity, thence, the fluorescence intensity measurements related to the samples of the Andersen impactor were plotted on the standard curve to determine the concentration of test particles on each stage.

2.5 Recovery and analysis of viroaerosols on solid media

Only bacteriophage λeyfp was used for this part of the study. Viroaerosols were generated and collected as described earlier, however, the collection medium for the Andersen impactor was modified to contain two ml of a 1.5% agar in distilled water medium evenly distributed on the bottom of each stage's Petri dish. The collection time was of 10 min between two 10 min monitoring periods using the APS. The viroaerosol impaction sites were analyzed under EFM using Nikon's Plan Fluor 4X and 100X magnification objectives. Image acquisition and processing was accomplished using the software mentioned above.

2.5.1 Fluorescence lifetime imaging microscopy (FLIM)

FLIM investigations were attempted in order to obtain better estimations of the viral recovery on solid media by eliminating possible background in samples and their preparations. The FLIM setup was a custom-build apparatus based on PicoQuant's time-resolved spectroscopy system, the MicroTime 200 (PicoQuant GmbH, Berlin, Germany). A picosecond pulsed diode laser from PicoQuant (LDH-D-C-485) was used as the exciting source combined to an Olympus IX-51 inverted microscope (Olympus America Inc., Center Valley, PA, USA) with a 60X magnification Olympus objective (UPLSAPO 60XW, NA 1.2). A multi-axis piezo-nanopositioning stage (P-517.3CL, Physik Instrumente, Irvine, CA, USA) was used to scan 150 x 150 pixel size images with a pixel size of 0.533 μm. A single photon avalanche diode (PDM Serie, PicoQuant) was connected to a PicoHarp 300 Time-Correlated Single Photon Counting (TCSPC) system for photon detection. PicoQuant's SymPhoTime and FluoFit softwares were used for data acquisition and for post-analysis, respectively. Prior to each experiment, the laser source was preheated and properly aligned using the appropriate Quantum dots dried on a microscope coverslip. Preliminary FLIM measurements were taken on dried liquid samples of virus models λeyfp and YG microspheres on either microscope coverslips or the 0.22μm MF-Millipore membranes that were used inside the IOM samplers. The FLIM measurements

were compared to culture media measurements in order to observe any differences between background signals and virus models.

2.6 Calculation of viroaerosol recovery

Relative recovery (RR) parameters were used in order to compare recovery efficiencies between the different viral models on the different stages of the Andersen impactor using the mentioned analysis methods. The RR defined in this paper derives from another previously used and described in a similar study [27]. It is defined as

$$RR = \frac{C_R}{\frac{Q_L C_N}{Q_{PA}}} \times \frac{Q_{PA}}{Q_{CA}} \tag{2.1}$$

which corresponds to

$$RR = \frac{C_R (Q_{PA})^2}{Q_L C_N Q_{CA}} \tag{2.2}$$

where C_R is the concentration of the sample recovered (PFU, genome copies or fluorescent particles per L of air), C_N is the particle concentration in the nebulizer solution (PFU, genome copies or fluorescent particles per ml of medium), Q_L is the nebulizer liquid flow rate (ml of medium per min), Q_{PA} is the aerosol flow rate produced inside the chamber (in this study, 33 L per min), and Q_{CA} is the aerosol flow rate collected by the sampler (in this study, 28.3 L per min). RRp is defined as the relative recovery determined by plaque assay, RRq as the relative recovery determined by qPCR and RRf as the relative recovery determined by fluorescence spectroscopy and microscopy.

2.7 Statistical analysis

All analysis were conducted using IBM's SPSS Statistics version 20 (IBM Corp., Armonk, NY, USA). Analysis of variances (ANOVA) were used to compare the different experimental factors: viral models (P008, PP01-GFP/SOC, λeyfp and YG Microspheres), types of analysis (qPCR, plaque assay and EFM), and the different stages of the Andersen impactor. If the normality assumption and homogeneity of variances of the data were not respected when using the *Shapiro-Wilk* test as well as the plots of predicted values and standard residuals, the nonparametric tests of *Kruskal-Wallis* and *Mann-Whitney U* for independent samples were used. All values were log transformed and the reported P-values were based on theses transformations. The results were considered significant with P-values ≤ 0.05.

Chapter 3

Results

3.1 Characteristics of virus models and viroaerosols

Table 3.1 describes various fluorescent characteristics for each virus model and figure 3.1 represents typical fluorescence microscopy images of the four models in samples from the nebulization medium. Using the system described in this study, the non-biological YG microspheres displayed greater fluorescence irradiance and area size per particle than the bacteriophage models. When comparing the fluorescence data between the three bacteriophages, P008-SYBR Gold had greater fluorescence irradiance and area size than PP01-GFP/SOC and λeyfp. However, even though λeyfp displayed inferior fluorescence irradiance and area size, it had a higher fluorescence count per area than the other two bacteriophage models but less than the YG microspheres.

Table 3.1: Experimental characteristics of the virus models in EFM.

Model	Relative fluorescence per particle	Experimental diameter of fluorescence particle (μm)	Relative fluorescence per μm^2
YG microspheres	11 ± 3	0.46 ± 0.04	17 ± 6
λeyfp	2.1 ± 0.5	0.136 ± 0.006	36 ± 10
PP01-GFP/SOC	1.2 ± 0.2	0.22 ± 0.02	8 ± 2
P008-SYBR Gold	3 ± 1	0.27 ± 0.07	13 ± 8

The size distribution obtained from the APS was expressed as delimited aerodynamic diameter channels equivalent to the d_{50} of particles trapped from stage one to six of the Andersen impactor (figure 3.2). For the four models investigated, similar particle size distributions were observed during triplicate aerosol generation experiments, however, greater numbers were obtained when aerosolizing the YG microspheres: a five-fold increase for the channels equivalent to stages three to smaller than six, and a 25-fold increase for channels equivalent to stages one and two. The mass median aerosol diameter (MMAD) of the aerosol obtained

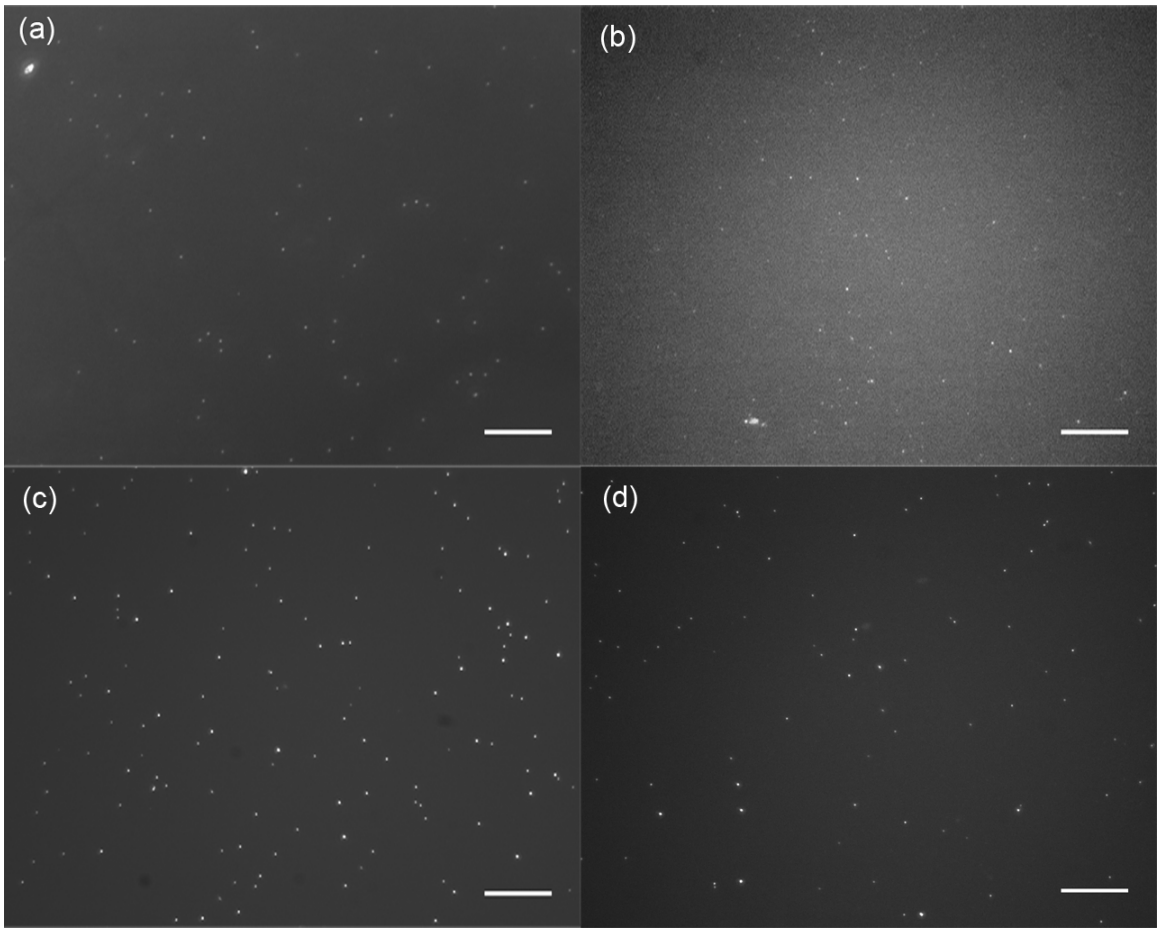

Figure 3.1: Images of the four virus models in the nebulization medium after aerosolization experiments: (a) P008-SYBR Gold, (b) PP01-GFP/SOC, (c) YG microspheres and (d) λeyfp. Scale bar: 10 μm.

after nebulization were of 0.94 $\pm$ 0.02 μm, and the total particle concentrations were 1.74, 1.92, 1.57 and 6.76, $\times$ 10^7 particles per L of air for P008, PP01-GFP/SOC, λeyfp and YG microspheres, respectively.

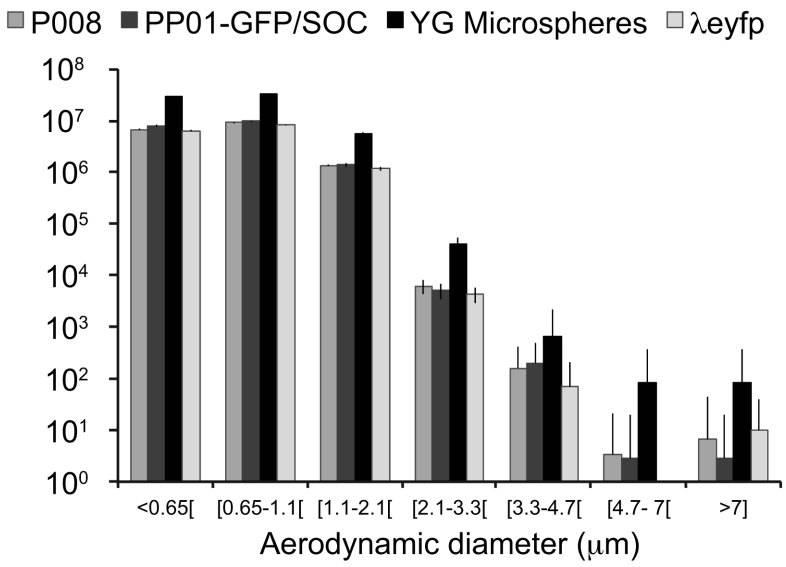

Figure 3.2: Particle size distribution obtained with the APS after generating viroaerosols for 10 min at 3 L per min for the four virus models in phage buffer (n = 3 for each virus model).

The temperature and relative humidity (RH) inside the chamber for the different aerosolizations conducted were of 27.3 ± 0.2 °C and 4.4 ± 0.5%, respectively. The quantity of viral models in the nebulization medium was measured by plaque assay, qPCR and EFM, and is presented in table 3.2. For phage P008, a 500-fold and 140-fold increase in quantification was observed when using qPCR compared to plaque assay and microscopy, respectively. Similar results were observed for phage PP01-GFP, a 10000-fold and 140-fold increase in quantification for the same comparisons. For λeyfp, no PFU were obtained after plaque assay and their was a four-fold increase between microscopy and qPCR for viral particle quantification. Furthermore, the total amount of liquid aerosolized was determined by measuring the remaining liquid in the nebulizer at the end of aerosol generation (liquid flow rate). During triplicate experiments, 0.09 ± 0.06 ml of nebulization medium per min were aerosolized for the four models.

Table 3.2: Virus model quantification in the nebulization medium prior to the experiments.

Model	qPCR (genome copies per ml)	Plaque assay (PFU per ml)	Fluorescence microscopy (particles per ml)
P008-SYBR Gold	$(2.6 \pm 0.4) \times 10^{10}$	$(5 \pm 3) \times 10^{7}$	$(1.8 \pm 0.2) \times 10^{8}$
PP01-GFP	$(2.6 \pm 0.9) \times 10^{10}$	$(2.7 \pm 0.5) \times 10^{6}$	$(1.8 \pm 0.4) \times 10^{8}$
λeyfp	$(7.3 \pm 0.5) \times 10^{7}$		$(3.2 \pm 0.8) \times 10^{7}$
YG Microspheres			$(3.7 \pm 0.5) \times 10^{10}$

3.2 Viral recovery from the Andersen impactor

Figure 3.3 and table 3.3 details the quantification of viral particles on the different stages of the Andersen impactor using the different analysis methods with their detection limits for the four virus models. No data was recovered from stages one and two of the Andersen impactor when using the three methods of analysis for all models and also, no fluorescence data was obtained from stages 3 and 4 for the three bacteriophage models. As it was for the quantification of λeyfp in the nebulization medium, no PFU were observed after aerosolization and aerosol collection.

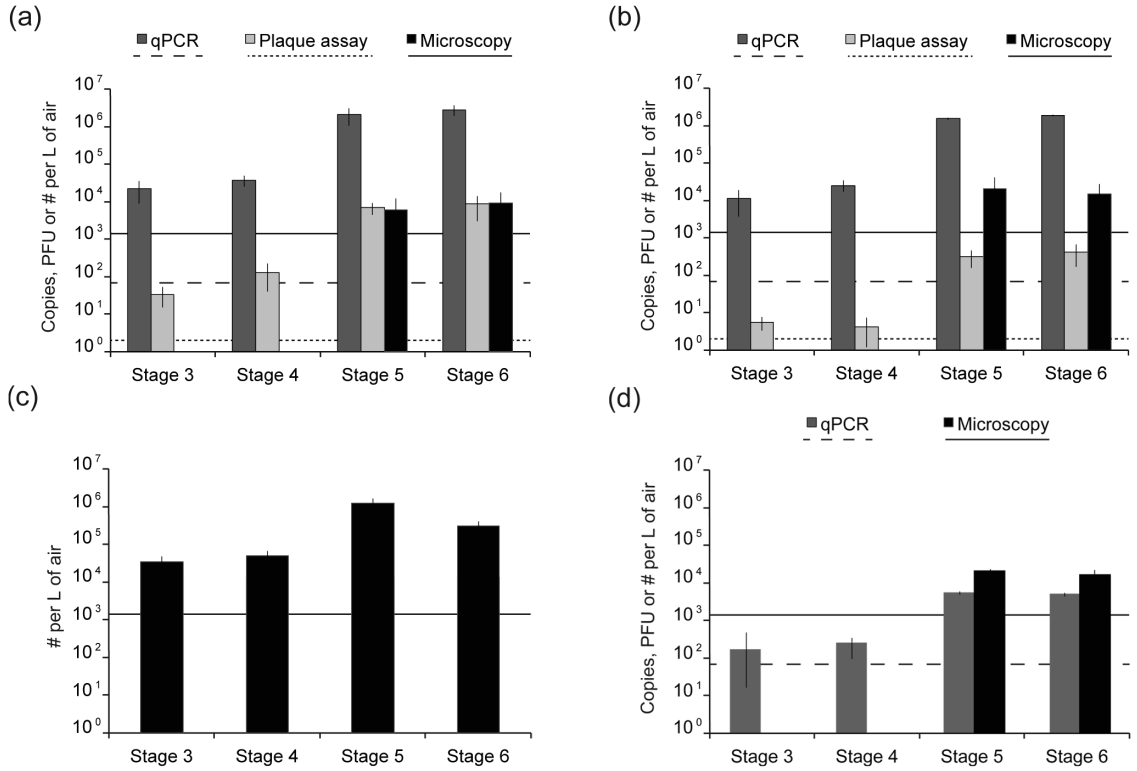

Figure 3.3: Comparison between qPCR, plaque assay and EFM for detecting and quantifying viroaerosols in liquid after a 10 min aerosolization at 3 L/min of the four models: (a) P008, (b) P001-GFP/SOC, (c) YG microspheres and (d) λeyfp. Lines represent the limits of detection for each analysis method in this study (n = 3 aerosolizations for each virus model).

3.3 Relative recoveries (RRs)

Figure 3.4 shows the recoveries of viral particles from the different stages of the Andersen impactor relative to the amount of viral particles aerosolized for the three models using the three analysis methods. No statistical differences were observed between the three bacteriophages models for viral recovery when comparing the different RRs. For the YG microspheres, a six-fold decrease of particle enumeration was observed when compared to the bacteriophage

Table 3.3: Viral recovery from the Andersen impactor.

Model	Stage	qPCR (genome copies per L of air)	Plaque assay (PFU per L of air)	Fluorescence microscopy (particles per L of air)
P008-SYBR Gold	3	$(2 \pm 1) \times 10^4$	$(3 \pm 2) \times 10^1$	
	4	$(4 \pm 1) \times 10^4$	$(1.3 \pm 0.9) \times 10^2$	
	5	$(2 \pm 1) \times 10^6$	$(7 \pm 2) \times 10^3$	$(6 \pm 6) \times 10^3$
	6	$(2.8 \pm 0.9) \times 10^6$	$(8 \pm 6) \times 10^3$	$(9 \pm 8) \times 10^3$
PP01-GFP	3	$(1.1 \pm 0.8) \times 10^4$	$(6 \pm 2) \times 10^0$	
	4	$(2.5 \pm 0.8) \times 10^4$	$(4 \pm 3) \times 10^0$	
	5	$(1.5 \pm 0.1) \times 10^6$	$(3 \pm 2) \times 10^2$	$(2 \pm 1) \times 10^4$
	6	$(1.87 \pm 0.09) \times 10^6$	$(4 \pm 3) \times 10^2$	$(2 \pm 1) \times 10^4$
λeyfp	3	$(2 \pm 2) \times 10^2$		
	4	$(3 \pm 2) \times 10^2$		
	5	$(8 \pm 1) \times 10^3$		$(3 \pm 2) \times 10^4$
	6	$(7 \pm 2) \times 10^3$		$(3 \pm 1) \times 10^4$
YG Microspheres	3			$(3 \pm 1) \times 10^4$
	4			$(5 \pm 2) \times 10^4$
	5			$(1.2 \pm 0.4) \times 10^6$
	6			$(3.1 \pm 0.9) \times 10^4$

models on stage 6 of Andersen sampler. No statistical differences were observed between qPCR, plaque assay and EFM when comparing the different RRs for viral recovery for the four models. Again, no statistical differences were observed between stages 5 and 6 of the Andersen impactor for plaque assay, qPCR and EFM when comparing the different RRs to each other for the four models except for stage 6 with the YG microspheres as mentioned above. On average, a 1.6-fold increase of RR was observed when comparing stage four to stage three for all models and analysis methods. A 90-fold average increase was also observed when comparing stages five and six to stage three, and a 50-fold increase when compared to stage four.

Figure 3.5 shows the RRs in respect to the number of particles observed with the APS for the different stages of the Andersen impactor for each virus model. No statistical differences were observed between the bacteriophage models. For the YG microspheres, decreases of 10-fold and 30-fold were observed for stages four/five and six, respectively. The RRs per particle are shown to follow approximately an inverse exponential function dependent to the stages of the Andersen impactor, which means that the number of viruses per particle is much higher on the lower stages of the sampler.

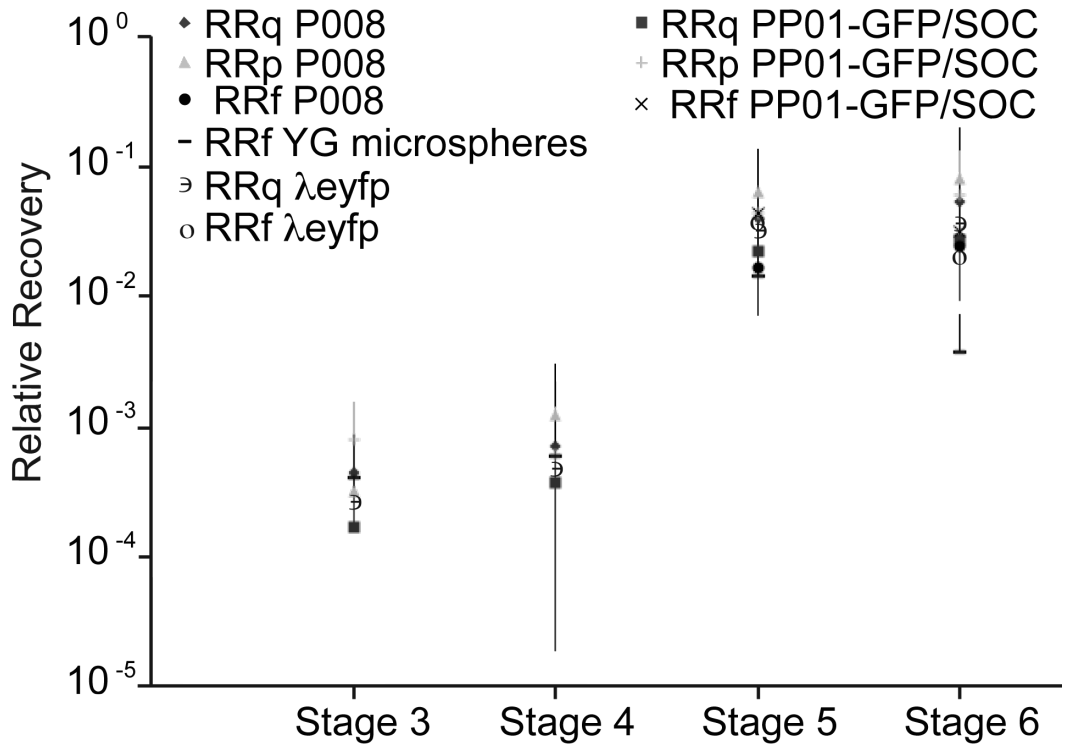

Figure 3.4: Relative recoveries calculated from plaque assay (RRp), qPCR (RRq) and EFM (RRf) of the four stages analyzed from the Andersen impactor for the four phage models (n = 3 aerosolizations for each virus model).

3.4 Single-laden viroaerosols

Figure 3.6 displays single particle viroaerosols recovered in liquid samples of the Andersen impactor. The majority of fluorescent particles recovered were between the geometric size range of single viral particles (approx. 0.3 μm) and approx. 10 μm. However, no size distribution has been produced since larger particles than the single viral particles were scarce.

Figure 3.7 displays typical microscope images of an impaction site on the solid agar medium from stage 6 of the Andersen impactor. Image (a) represents an entire impaction site (one of 400 on each stage) observed using a 4-fold magnification in EFM, and (b) represents the same impaction site observed at a 100-fold magnification. Estimations of the number of viruses per impaction site were calculated by averaging the sum of fluorescent particles near the edge of the impaction site with those near the center at 100X magnification. The areas analyzed using the images taken at 100X magnification (5884 μm^2) were then added up to the fraction remaining of the entire impaction site (approx. 700 μm in diameter). The average of fluorescent viral particles recovered per impaction site was of $2 \pm 1 \times 10^6$ corresponding to $6 \pm 5 \times 10^3$ fluorescent viral particles per L of air collected on stage 6.

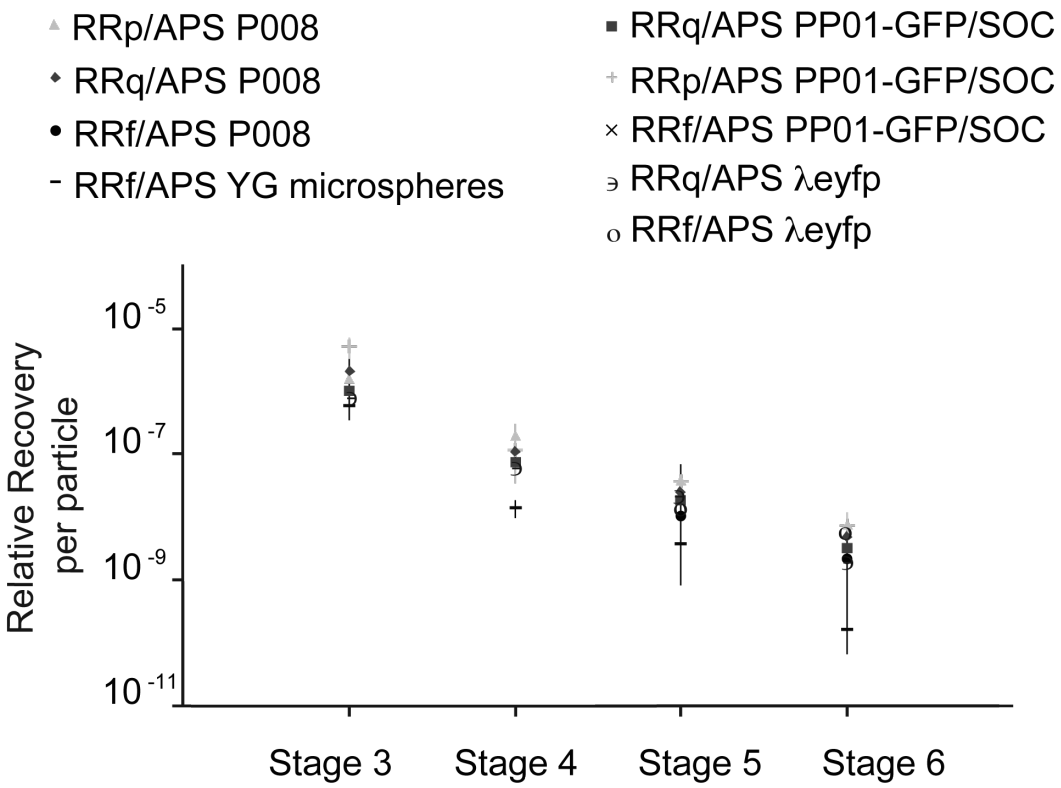

Figure 3.5: Relative Recoveries calculated from plaque assay (RRp), qPCR (RRq) and EFM (RRf) in respect to the number of particles observed with the APS for the four stages analyzed from the Andersen impactor for the four phage models (n = 3 aerosolizations for each virus model).

3.5 FLIM

Figure 3.8 shows an example of an image obtained in FLIM for the (a) YG microspheres and (b) λeyfp model. After analysis of preliminary FLIM data of the two tested virus models on either the microscope coverslips or the 0.22μm MF-Millipore membranes, no discernible differences were observed between the virus models and the dried culture media. For this reason, FLIM experimentations on air samples were not attempted.

3.6 Fluorescence spectroscopy

Fluorescence spectroscopy was performed first on λeyfp model. The spectroscopy results from different dilutions were then paired to EFM counts of the same dilutions in order to estimate a number fluorescence particles for the fluorescence obtained in spectroscopy (figure 3.9). After further investigations, fluorescence spectroscopy analysis was discarded because the culture media used (TSB) emitted strong fluorescence signals at same wavelengths as the bacteriophage models (figure 3.10) when excited at 488 nm.

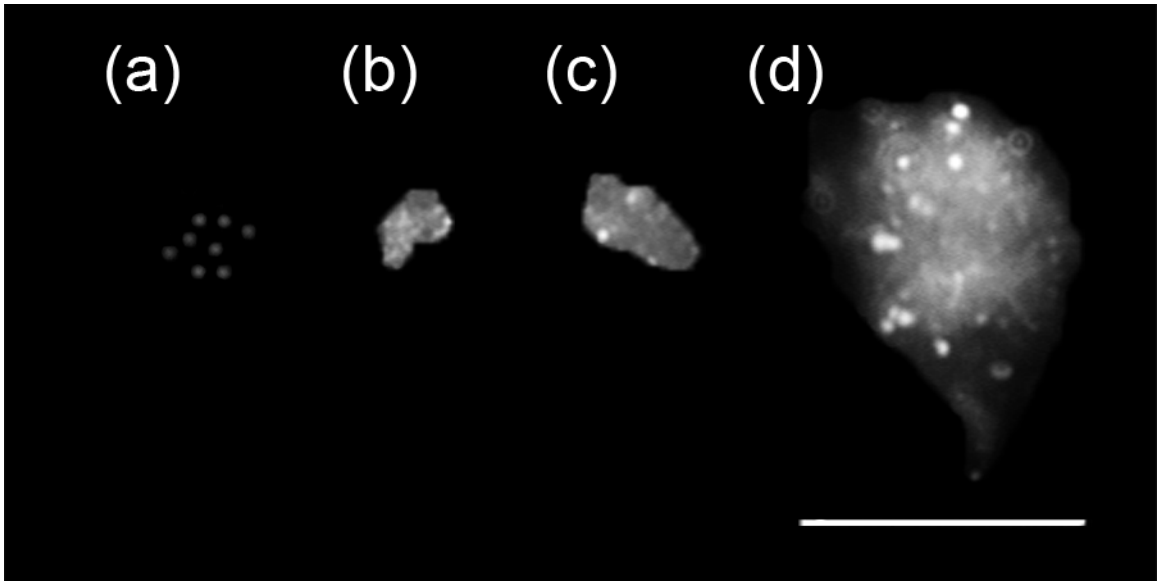

Figure 3.6: Fluorescence microscopy images of different sizes of viroaerosol aggregates recovered from different stages of the Andersen impactor for the bacteriophage models: (a) single viral particles, (b) to (d) aggregates of viroaerosols. Scale bar: 10 μm.

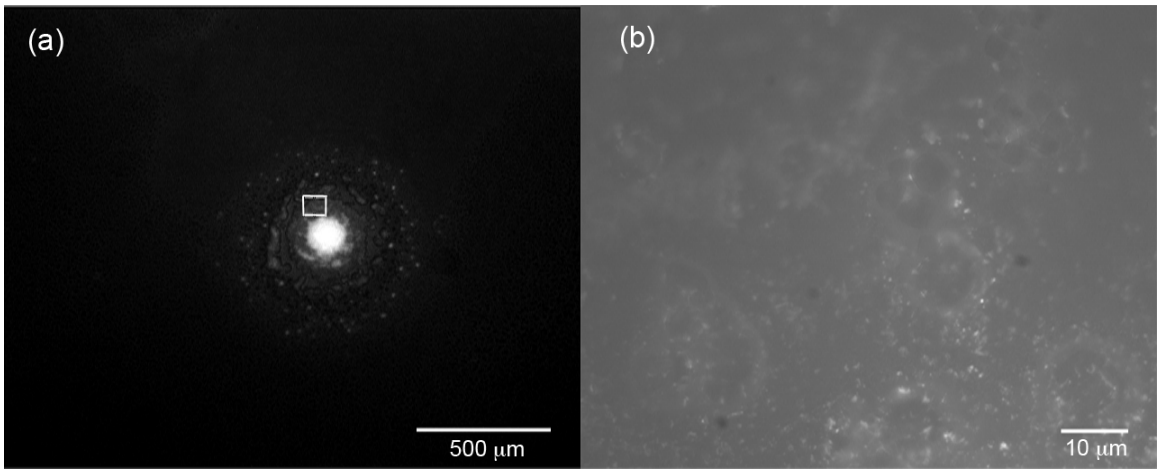

Figure 3.7: Epi-fluorescence images of λeyfp viroaerosols collected in the solid agar medium of stage 6 of the Andersen impactor: (a) represents an image taken at a 4X magnification of an entire impaction site, the area surrounded in a white rectangle represents (b), an image taken at a 100X magnification.

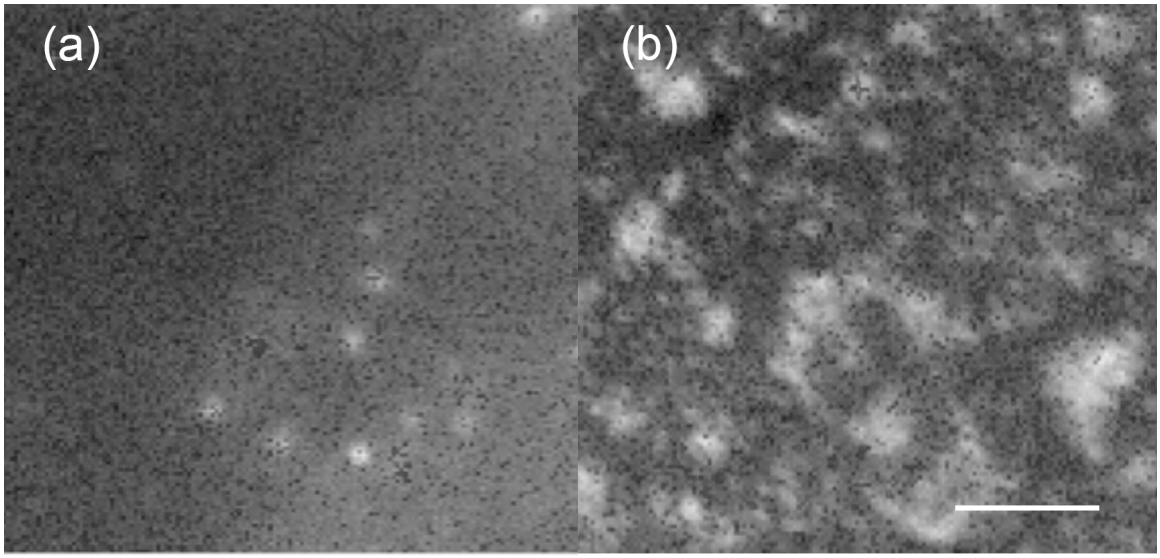

Figure 3.8: FLIM images of virus models: (a) YG microspheres and (b) λeyfp air-dried on microscope coverslips. Scale bar: 10 μm.

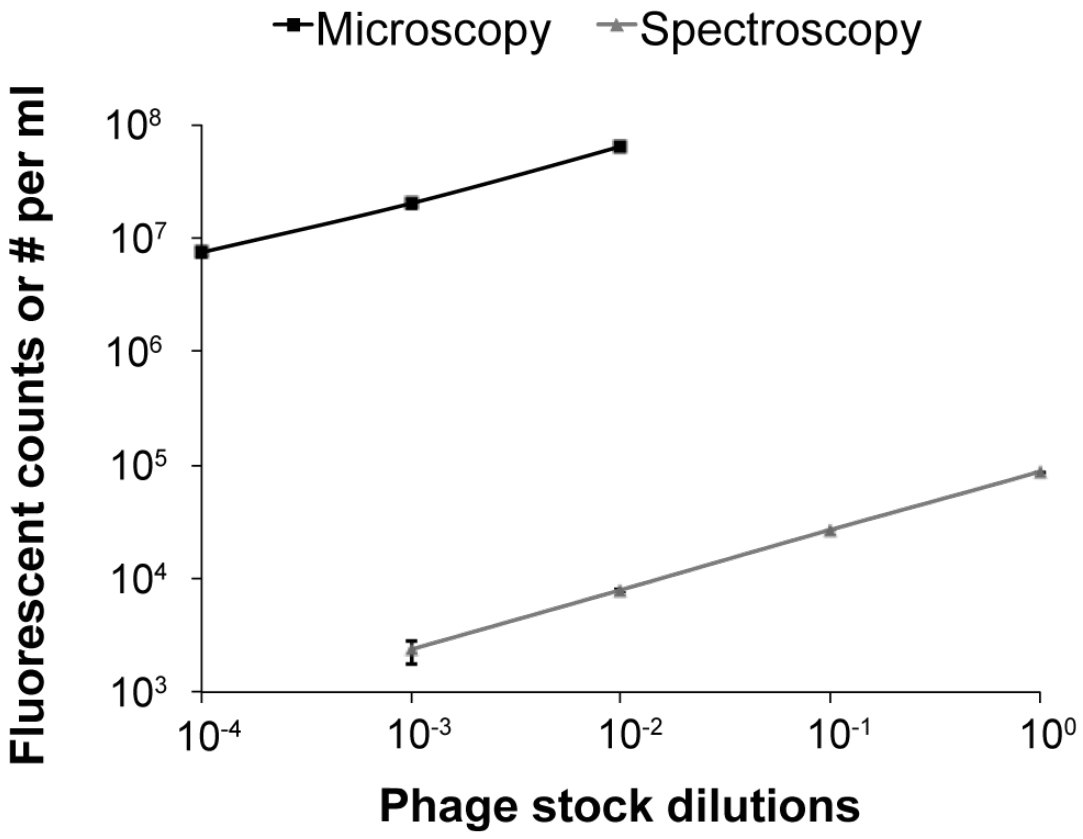

Figure 3.9: Comparison of fluorescence spectroscopy and EFM for detecting and enumerating λeyfp on bacteriophage stock samples. Dilutions were prepared with phage buffer.

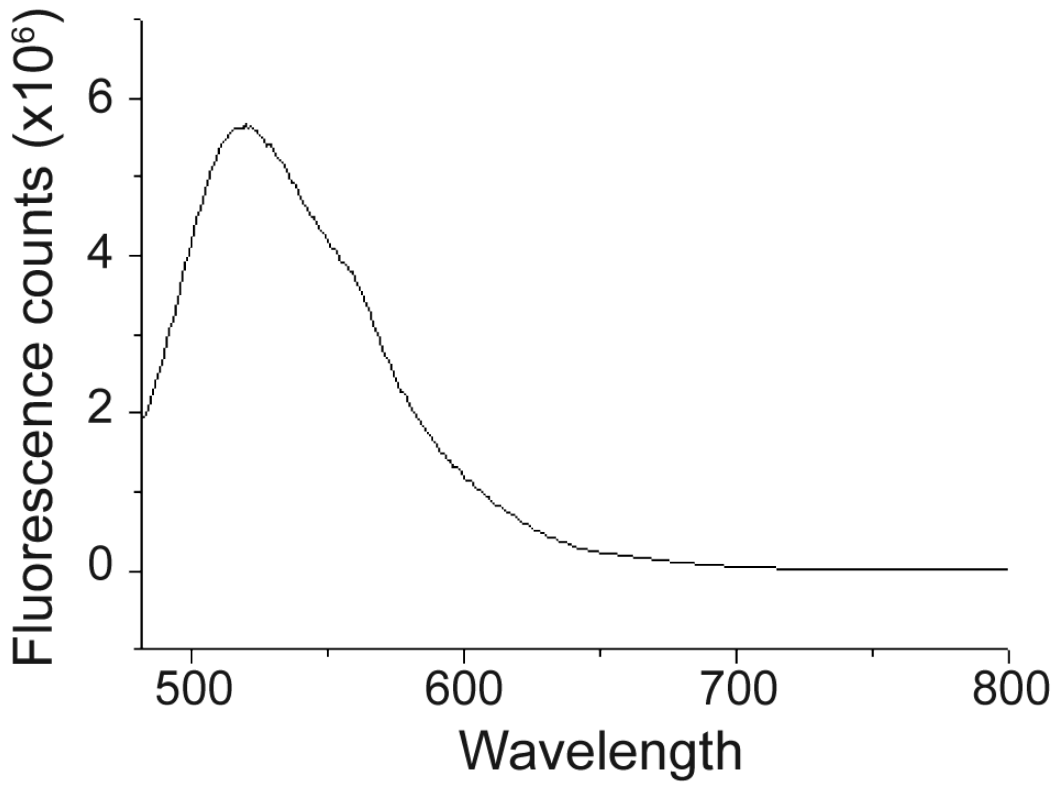

Figure 3.10: Fluorescence emission spectrum of the TSB culture medium used for the preparation of λeyfp and PP01-GFP bacteriophage models when excited at 488 nm.

Chapter 4

Discussion

4.1 Concentration and size distribution of viroaerosols

The concentration and size distribution of the aerosol generated was chosen to offer an interesting size range in order to study characteristics of virus-laden particles. While the concentration of particles is high ($>10^6$ per min), the size distribution determined by the APS happens to be comparable to the size distribution of cough-generated aerosols produced by Influenza patients (average of 0.63 μm count median diameter) [42]. The size distributions and MMADs for the bacteriophage models tested here are practically identical such as demonstrated in figure 3.2. Given the fact that the viroaerosols were created from the same mixture (phage buffer), except for the differences of medium in which the virus models were cultured, it was expected that the particle size distributions would be equivalent. To support this assumption, it has been established that the presence of bacteriophages has little influence on the size distribution of a nebulized suspension [32]. Furthermore, in comparable studies using the same system, similar concentrations and size distributions were obtained with other bacteriophage models: MS2, ϕ6 and ϕX174 [27, 71]. Interestingly, the YG microsphere had a slightly different distribution for particles larger than four μm in aerodynamic size. This could be explained by the fact that its nebulization medium did not contain any culture medium and furthermore, the stock sample of microspheres contained different components that were not found in the nebulization medium used for the bacteriophages. The majority of virus model particles were detected on stages five and six of the Andersen sampler corresponding to aerodynamic diameters of particles between 0.65 and 2.1 μm. This concurs with the data reported by the APS revealing that most of the particles were observed between these aerodynamic diameters. Interestingly, in a similar study using a different aerosolization setup and bacteriophage model (MS2), the same phenomenon was described: a UV-APS showed that the majority of wet and dry droplets produced from the aerosolization of an artificial mucous suspension or a PBS suspension were of aerodynamic diameters from less than 0.5 to 2.1 μm, and that the majority of viruses collected were from the last two stages of the Andersen impactor [54].

4.2 The Andersen impactor for recovery of viroaerosols

The six-stage Andersen sampler is a cascade impactor capable of collecting aerosols according to their size distribution (see Material and Methods). The physical collection efficiency has been previously reported to be practically 100% under controlled conditions in a wind tunnel using non-biological, monodispersed aerosols of aerodynamic diameters up to 23 μm when very low wind speeds were used [69]. In this study, the relative recovery of viroaerosols for the Andersen impactor was between 2 and 13%, depending on the analysis method. For this particular system, the absolute collection efficiency cannot be determined because losses during aerosolization and sampling cannot be quantified and moreover, a large proportion of the aerosols created had an aerodynamic diameter smaller than the 50% cut-off size of the last stage of the impactor. However, when comparing the total relative recoveries of the six-stage Andersen impactor to the recoveries obtained while using polycarbonate and polytetrafluoroethylene filters combined to quantitative reverse-transcription polymerase chain reaction (qRT-PCR) with other bacteriophage models, similar outcomes were observed [27]. In addition, the six-stage Andersen impactor had higher infectious viral load relative recovery when analyzed using plaque assay in this study compared to the filters used in the previous research suggesting that the Andersen sampler could be less damageable to viroaerosols. Likewise, Tseng and Li concluded that a one-stage Andersen impactor had a 10-fold higher relative recovery than a nucleopore filter for the sampling of different bacteriophages using infectivity assays [66]. One problem occasionally encountered while using the Andersen impactor is the possible loss in viability or infectivity caused by the impaction of aerosols onto solid-surface media. However, as demonstrated here, the use of a liquid medium did not affect the recovery of infectious viruses. In fact, the liquid medium offered the advantages of direct analyses in qPCR and filtration of particles for microscopy analysis. Others have also opted for an aqueous medium to collect viroaerosols with the Andersen sampler: Tseng and Li [66] used Luria-Bertani broth (culture medium) with 3% gelatin plates, and Russell et al. [59] placed sterile mineral oil into Petri dishes on each stage of the impactor. On the other hand, a liquid medium has the disadvantage of evaporating during sampling thus inducing a lost of the given analyte. All considered, the six-stage Andersen impactor offers a variety of advantages, such as, separating aerosols according to their aerodynamic diameter, and allowing the use of various collecting media for different analysis procedures. It is not surprising that the Andersen impactor has been recommended in the past as a standard for recovering airborne microorganisms included those found in low concentrations [14]. Therefore, the Andersen impactor would be a great sampler not only for chamber studies but also for field research where concentrations of airborne viruses are not as abundant. Nevertheless, the choice of air sampler ultimately depends on the desired objectives to fulfill.

4.3 Comparison between analysis methods for viroaerosol quantification in liquid samples

When comparing relative recoveries of qPCR, plaque assay and EFM, equivalent results were obtained (figure 3.4). However, the sensitivity and specificity of each method differs greatly. For qPCR, higher numbers were detected compared to plaque assay and EFM. Also, fewer variations between the samples were observed using this technique. When comparing qPCR data to those of the plaque assays, the majority of phages used were non-culturable prior to aerosolization: 99.99% for PP01-GFP/SOC and 99.8% for P008. This outcome was also consistent with similar studies using different phage models in the same system [27, 71]. Furthermore, it has been shown that a large proportion (>68%) of qPCR signal from λ phage lysates was from free DNA, and suggested that accurate determinations of functional phage titers via qPCR required a prior DNase I treatment [22]. Consequently, a significant drawback of using qPCR for quantifying airborne microorganisms is that the infectivity of the given organism remains unknown. Moreover, the cost related to the devices needed for qPCR are greater than the costs of the accessories used in plaque assays. However, qPCR analysis requires less time to perform, a couple of hours, compared to culture periods of 18 to 24 hours needed for plaque assays.

The sensitivity of the plaque assays was found to be greater than the other two methods, however, the variability between replicates was also greater. This variability could maybe be explained by the inexperience of the manipulator. Moreover, plaque assays can only detect culturable viral particles limiting detection only to the infectious load of viroaerosols limiting the sensitivity of the assays compared to qPCR. As indicated earlier, between 0.2 and 0.01% of the tested phages were culturable compared to their genome copies implying that more targets would be available for detection using qPCR, hence, in an environment were viral concentration is low, qPCR would be more suitable to detect and quantify airborne particles. Others have also determined that qPCR was superior to plaque assay for the quantification and detection of phages and that the efficiency of qPCR could be improved by approximately 10% with the right set of primers [22].

For EFM on liquid samples, sensitivity was inferior when compared to the other two techniques. For the bacteriophage models, it was only possible to detect and quantify fluorescence signals on stages five and six of the Andersen sampler. Therefore, this method would not be useful when analyzing low concentrations of viroaerosols. However, virions that cannot be cultured are nevertheless visualized in EFM and thus, more accurate viral particle quantification can be assessed. EFM has been rarely compared to plaque assay or qPCR for viral quantification, Paul et al. have obtained 1.4-fold higher concentrations of T2 bacteriophage in artificial sea water when using 4' 6-diamidino-2-phenylindole (DAPI)-stained samples coupled to EFM compared to traditional plaque assay [53]. In this study, the viral quantities determined in

SYBR Gold-stained samples of phage model P008 were slightly higher (three-fold) in the nebulizer medium when compared to plaque assay, however, no differences were observed between the two methods when analyzing stages five and six of the Andersen impactor. For PP01-GFP, between 35- and 70-fold higher concentrations were observed in the nebulizer medium and the stages analyzed. These higher concentrations detected in EFM could be due to viroaerosol aggregates present in the nebulization medium before or after aerosolization. Aggregates that can be observed by EFM cannot be determined by plaque assay. Furthermore, EFM has been shown to have higher fidelity than transmission electron microscopy (TEM) and flow cytometry (FCM) for enumerating virus-sized particles when comparing accuracy errors between techniques (EFM error: 0%, TEM and FCM: 8%)[26].

Altogether, the sensitivities of the analysis methods performed in this study fundamentally depend on the volumes of the samples used for analysis. For qPCR, only a small amount of the sample is used, 0.025% (5 μl of 20 ml per Andersen stage) compared to 0.5-5% for plaque assay and 5% for EFM. However, the whole amount used for analysis is quantified, and the same is valid for plaque assays, compared to EFM, where the 5% of sample analyzed is also fractioned by the field of view of the lens system. In this case, only an area of 0.006 mm^2 out of an area of 130 mm^2 of sample filtered can be viewed at a time, meaning that only 0.0002% of the sample can be analyzed at once after image acquisition. It would be possible to improve the detection limits by using greater volumes of samples, however, the techniques would not necessarily permit the addition of more sample volume. For qPCR, this would affect the salt concentrations and could deteriorate the expected results. Changing salt concentrations has been shown to change the viable titer of phage T2 preparations a 1000-fold [15]. For EFM, the amount of liquid to be filtered in order to get a 10-fold increase of detection limit would exceed the practical time for analysis if multiple samples would be done. On average, a three to four-minutes filtration period was needed with one ml of sample. Another way to improve the detection limit of the EFM system would be to use an objective offering a larger field of view (a lower magnification) without loosing any spatial resolution (very high numerical aperture (NA)).

The specificity of qPCR for the detection and quantification of virus samples is very accurate when using the appropriate gene-specific primers, however, precautions are needed in order to minimize the possible occurrence of false negatives and false positives. The software used for qPCR was capable of fluorescent melting curve analysis allowing differentiation of non-specific amplification products that usually cause confusion while interpreting results. Analysis of amplicon melting curves has shown that the sensitivity of SYBR green 1, the DNA-binding fluorophore used in this technique, is decreased by non-specific amplification at low initial target template concentrations [45]. Here, the initial target template concentrations of 5 to 50 copies per reaction were clearly distinguishable from non-specific background amplification (data not shown), thus, the detection limit of the qPCR analysis method was dictated by

these low initial concentrations. Furthermore, a variety of known inhibitors, such as calcium, hematin, melanin, humic acid, collagen, indigo and tannic acid can affect PCR reactions to create false negative. qPCR for quantifying airborne microorganisms is that the infectivity of the given organism remains unknown [51]. While these inhibitors may be commonly found in aerosol samples from field research, the can be easily controlled in laboratory chamber studies. For plaque assay, this traditional cell culture method is highly host specific, however, if samples are not treated properly: extended contact-time with heated agar or vigorous shaking disrupting the structures necessary for viral infection, lesser numbers would be detected. The use of a fluorescent-expressing virus couple to EFM is very specific when the components used for aerosolization are known. For chamber studies, it is fairly easy to use non-fluorescent components in the aerosolization system that could be otherwise mistaken for viral particles when analyzed. Furthermore, if impossible to eliminate all unwanted fluorescence background in a system, it should be possible to use another viral model expressing a different fluorescent protein to better differentiate unwanted fluorescence signals from those emitted by viruses. The less specific method would be the use of the fluorescence DNA-binding dye SYBR Gold that can bind, not only to the viral DNA encapsulated inside virions but to all free DNA in samples. However, as shown in this study, no differences were observed when using this technique when enumerating viral particles compared to the others, suggesting that the fluorescence signals from non-viral particles, if any, would be negligible when using the setup presented here.

For fluorescence spectroscopy, it would have been a great analysis method for its rapid use and quantification if the virus models would have produced greater fluorescence signals than the background signals in samples. Compared to EFM, it was not possible with this spectroscopy setup to filter the samples and get rid of the majority of unwanted signals. As shown previously, the culture medium used to produce the bacteriophage lysates produced high fluorescence signals. For this reason, a new culture medium was tested at the end of this study with the λeyfp bacteriophage model: minimal glucose medium [11]. While the minimal glucose medium produces a minimal fluorescence signal in the range of interest in this study (data not shown), it was however impossible at this time to obtain viruses from these cultures. This could be caused by the lack of expression of the recombinant λeyfp prophage in the *E. coli* host cells that need optimal conditions in order to properly be produced [46]. The next step would have been to use this minimal medium with the PP01-GFP model or use purified phages, however, time did not permit it.

4.4 Quantification of viruses on single aerosol particles and solid media

The principal aim of this study was to verify the possibility of analyzing viruses on single aerosol particles using new models and techniques. As shown previously, it was possible

by using fluorescent models combined with EFM to visualize and quantify viruses on single aerosol particles. Furthermore, an advantage of using a fluorescent model is the possibility of analyzing the airborne samples at the particle level on solid media with minimal disturbance of the aerosols after recovery. Compared to other methods used in previous studies, such as, aerosol collection using filters [27, 71] where less than 50% of viruses are recovered after elution of aerosol particles from the filter apparatus (unpublished data). Not only that the aerosols are less disrupted but information on how they are gathered in or on the collection medium is possible by using EFM with a fluorescent model. Such was the case with the Andersen impactor in this study where visualization and analysis of undisturbed viroaerosol impact sites was done. However, it was unclear if the fluorescent signals analyzed were coming from the viruses or a mixture of the models and the culture media that, as mentioned earlier, could not be eliminated from the process. Nevertheless, when comparing data obtained from virus model λeyfp on stage 6 of the Andersen impactor using the analysis method in liquid samples with the preliminary data from the method used on the solid medium, similar results were obtained. No statistical analysis could be done because of the lack of tests done on the solid media. An interesting method that could have overcome the problems encountered by the background fluorescence signals could have been the FLIM technique. However, after treating and analyzing preliminary data from the FLIM experiments, it was very difficult to interpret fluorescence signals coming from the samples. First, the medium was extremely complex and in addition to having an uneven surface that was unsuitable for proper analysis, the fluorescence signals from the culture media could not be differentiated from the models and background signals. FLIM is a powerful tool but also has its limitations, such as, subtracting components of a given signal, and therefore, besides having a highly performing system, a highly experimented manipulator is required. The experiments attempted here, in addition to being performed on a complex matrix, are done at the nanoscopic level, which increases the complexity of the manipulations and analysis.

4.5 Comparison of the fluorescent viral models for aerovirology investigations

Interestingly, the efficiency in terms of fluorescence irradiance per μm for each model followed the same relation as the brightness defined in table 1.1. However, this association is not fully adequate because the data acquired in this study was done using non-optimal instrumentations: the FITC filter set of the epi-fluorescence microscope had poor excitation and emission spectra for models PP01-GFP, λeyfp and the YG microspheres. In addition, the number of fluorophores per virion were different between bacteriophages and unknown for the YG microspheres. Nevertheless, the YG microspheres were found to be more efficient in terms of fluorescence irradiance and area size compared to the bacteriophage models. Also, the stock solution of microspheres contains greater numbers of particles per volume than the prepara-

tions of bacteriophages given the advantage of working with high concentrations in aerosols. However, microspheres have the disadvantage of being non-biological, hence, they cannot give any information on viral structural damages nor on the infectivity of airborne viruses in any case. Furthermore, the results demonstrated here suggest that the microspheres react differently than the bacteriophage models when aerosolized and recovered, however, this could be due to the differences in the nebulization medium and not because of the model itself. Bacteriophage P008 stained with SYBR-Gold and λeyfp offered better fluorescence characteristics than bacteriophage PP01-GFP/SOC. The main advantage of using nucleic acid dyes for staining viruses is that it can be done on a great number of virus species. Moreover, it has been shown to provide good estimates of virus abundance in water and culture samples [75] and, SYBR Gold was describe as a good choice for the majority of samples [52]. However, it has the disadvantage of staining free nucleic acid as well, such as, bacterial DNA fragments, aggregates of free DNA or even unwanted viral DNA. The staining also adds a supplementary step prior to analysis compared to a fluorescence-expressing model. For λeyfp, lower concentrations were obtain in qPCR compared to the other two phage models and lower concentrations of phages were quantified from the lysates for qPCR and EFM as well. Plaque assay did not work under the conditions presented in this study so no information on the lost of infectivity after aerosolization could be obtained. Another difference encountered with the λeyfp model was that when comparing qPCR data to EFM data for viral quantification, more than 100% of the qPCR data could be visualized in microscopy compared to less than 1% for the other two phage models. This difference as well as the problems confronted in plaque assay may be due to the fact that λeyfp is a lysogenic phage compared to the other two that are lytic phages. An advantage of using the λeyfp model was having the higher contrast between viral signal and background fluorescent signals permitting visualization on solid medium. The fainter signal obtained from PP01-GFP did not permit proper differentiation between the background medium and the virus model. Like PP01-GFP, λeyfp has the main advantages of having viral structures, fluorescent by nature and still remains infectious. In a previous study, a fluorescence-expressing virus model was also used to study viroaerosol characteristics [41], however, the virus carried a GFP gene that could be expressed uniquely in the host cells allowing determination of the infectious load of the samples but not the visualization of the virus itself. The advantage of using the genetically modified virus models presented here is that they express fluorescent proteins on their capsids permitting detection and quantification regardless of its infectious potential.

Conclusion

We have used fluorescent bacteriophage models coupled with EFM to enumerate and quantify virus particles from aerosols. Our results suggest that the use of a fluorescence-expressing bacteriophage would be a great model to use in aerovirology studies interested in the overall characteristics of viroaerosol samples and also in the single particle analysis. We showed that the fluorescent phage models tested here had similar general aerosol characteristics (size distribution and MMAD) when compared to non-fluorescent phages evaluated in previous studies. The six-stage Andersen impactor was shown to preserve the infectivity of our virus models and correlations were attained between the sampler's aerodynamic separation and the size distribution obtained from a time-of-flight apparatus, an APS. Despite the fact that EFM is less sensitive than qPCR to detect viruses in aerosols, it was shown to be comparable to qPCR and plaque assay for quantifying fluorescent viroaerosols in liquid samples. Also, as mentioned previously, EFM is fast, reliable and can possibly be used to analyze single viral-laden particles on solid medium. However, in this study, not enough data was obtained in order to properly evaluate the use of EFM on solid media. Future investigations should be continued using models expressing improved fluorescent proteins to enhance brightness and to produce different fluorescence signals than the background in samples. Moreover, an animal virus model could be genetically engineered to express a fluorescence protein on its capsid that would allow the imaging of a complete viroaerosol infection in a living organism.

Annexe A

Matlab code for image analysis

The lines of code used to analyze images are shown on the next page. Briefly, images were loaded and displayed inside the Matlab program. After using the *find_particle* function with the desired values, the total fluorescence intensity and area size per particle was obtained and used for further analysis. An example of using the code is also described further below.

```
function [Data_particles outMean outArea outSum] =
find_particle(image,pixel_size,max_size,min_size,axes_handles)

Bg = imcrop(axes_handles);
Bg = mean(Bg(:));
im = filter2(ones(1,1),image-Bg);
%h1 = figure(100);imshow(im,[]);
level = 0.1;%graythresh(im/(max(im(:))))
BW = im2bw(im /(max(im(:))), level);
label_im = bwlabel(BW);
%h2 = figure(200);imshow(BW);

 STATS = regionprops(label_im,
image,'BoundingBox','PixelIdxList','Centroid','Eccentricity','Image','MeanIntensity','Area',...
     'FilledArea', 'FilledImage', 'PixelList','PixelValues');

 n=0;

 PSF_for_deconv = [];

 for i = 1:size(STATS,1)
   if STATS(i).Area < (max_size/pixel_size)^2  && STATS(i).Area > (min_size/pixel_size)^2
      n=n+1;
      Data_particles.MeanIntensity(n) = STATS(i).MeanIntensity;
      Data_particles.Area(n) = STATS(i).Area;
      Data_particles.SumPixelValues(n) = sum(STATS(i).PixelValues);
      Data_particles.Eccentricity(n) = STATS(i).Eccentricity;
      Data_particles.BoundingBox(n).ul_corner__width = STATS(i).BoundingBox;
      Data_particles.PixelIdxList(n).list = STATS(i).PixelIdxList;
      Data_particles.Centroid(n).xy = STATS(i).Centroid;
      Data_particles.Image(n).im = STATS(i).Image;
      Data_particles.FilledArea(n) = STATS(i).FilledArea;
      Data_particles.PixelList(n).list = STATS(i).PixelList;
          %axes(axes_handles)
          hold on axes_handles
          rect = [STATS(i).BoundingBox(1)-5,STATS(i).BoundingBox(2)-
5,STATS(i).BoundingBox(3)+10,STATS(i).BoundingBox(4)+10];
          plot([rect(1),rect(1)+rect(3),rect(1)+rect(3),rect(1),rect(1)],...
             [rect(2),rect(2),rect(2)+rect(4),rect(2)+rect(4),rect(2)],...
             'tag','plot','color',['r'])
          hold off
   end

  end

% L1=Data_particles.MeanIntensity;
% figure(1);hist(Data_particles.MeanIntensity,25)
% figure(2);hist(Data_particles.Area*pixel_size,25)
outMean = Data_particles.MeanIntensity';
%outArea = (Data_particles.Area)'.*pixel_size;
outArea = sqrt(Data_particles.Area)';
outSum = Data_particles.SumPixelValues';

end
```

Example of using the code

Reading and showing the image

Matlab command:

```
i=imread('image.tif');
imshow(i)
```

where *i=imread('image.tif')* is used to load an image and to assign the name i to it. The command *imshow(i)* is used to display the image loaded and is necessary for further analysis.

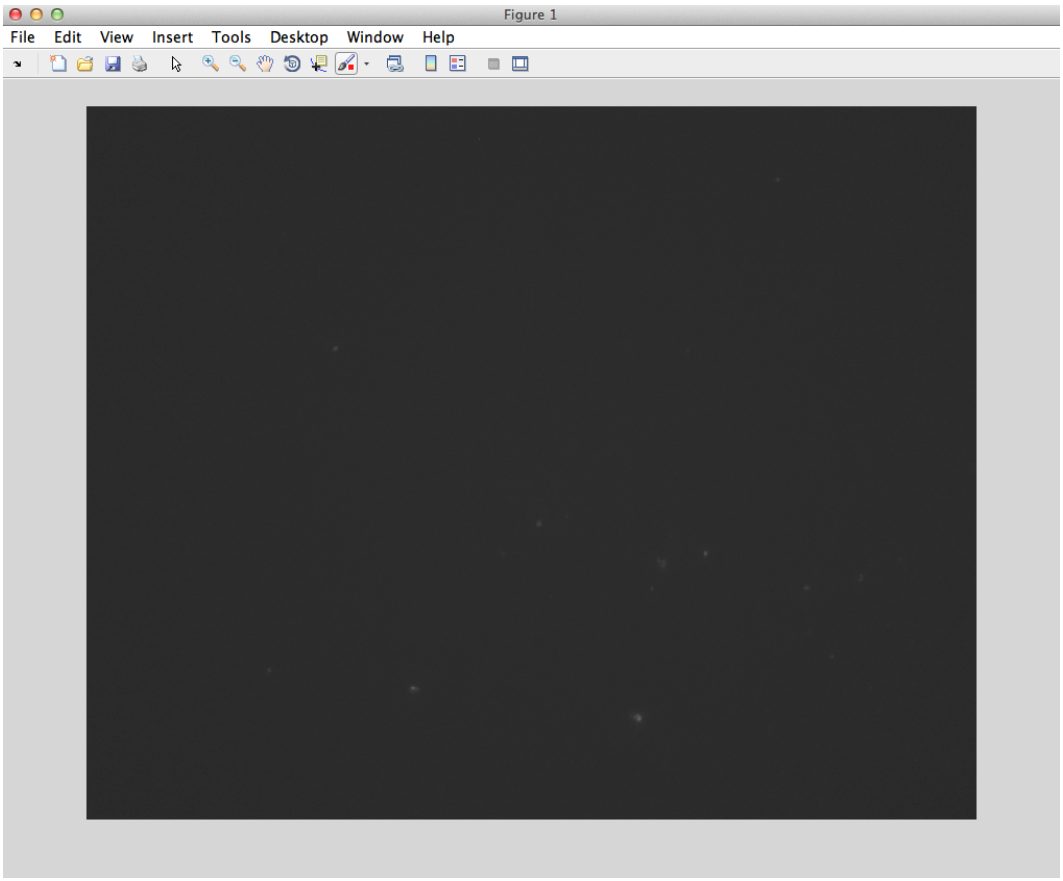

Figure A.1: Example using the Matlab procedure on a fluorescent microscopy image obtained from the methods described earlier of a sample of PP01-GFP/SOC phage model recovered on stage six of the Andersen impactor. Image is the result of the *imread* and *imshow* functions.

Particle analysis function

A threshold of 0.55 was used to eliminate the unwanted pixels during the analysis function. If unwanted particles were still observed after the analysis function, they were eliminated during the later calculations.

Matlab command:

[Data_particles outMean outArea outSum] = find_particle(i,67,100000000,67,1)

where, *Data_particles* is the particle analysis function, *outMean* is the average fluorescence signal per pixel in an area define by *Data_particles*, *outArea* is the total area size of a particle define by *Data_particles*, and *outSum* is the total fluorescence signal per area define by *Data_particles*.

Inside the *find_particle* function, the first value, *i*, is the image name, the second value,

67, is the pixel size in nm, the third value, *100000000*, is the maximum area size for a particle, the fourth value, *67*, is the minimum area size for a particle, and the fourth value, *1*, is given for the *axes_handles*.

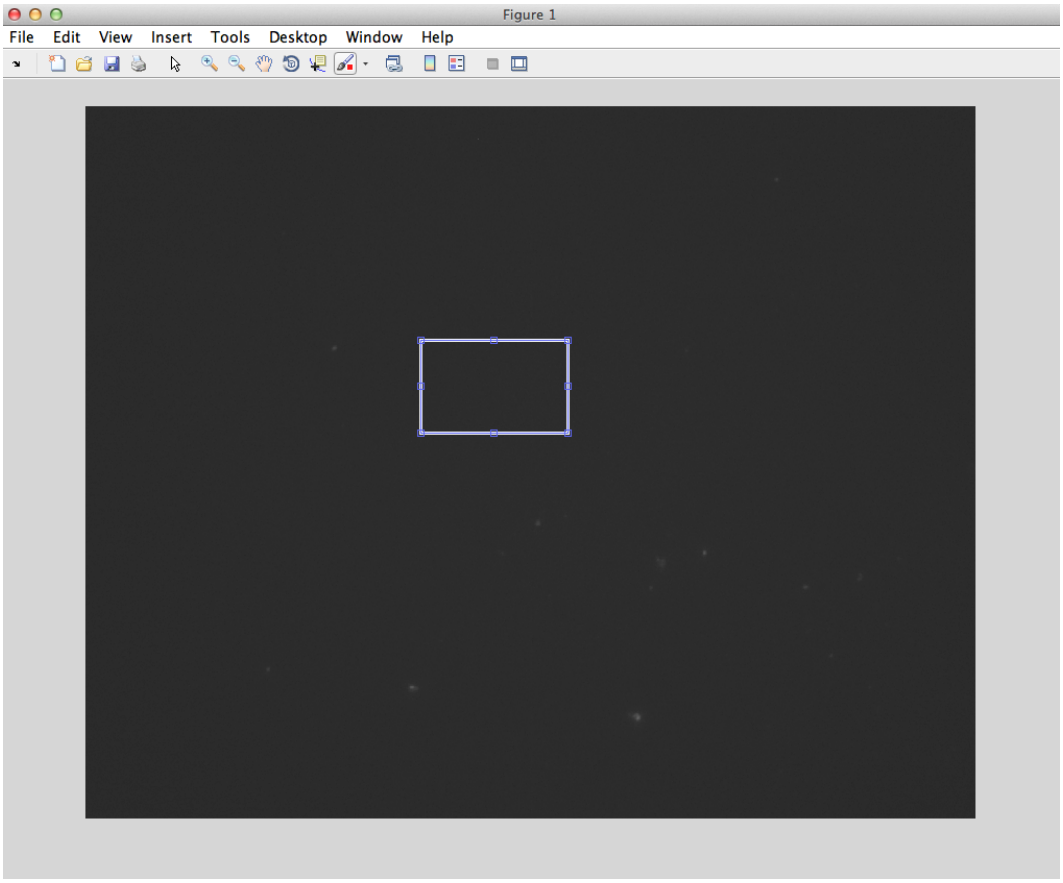

Figure A.2: The user is demanded to select a background for proper particle determination.

Data output

The data of the *outMean*, *outArea* and *outSum* are presented in the command line window, and copied to a Microsoft Excel sheet for further analysis.

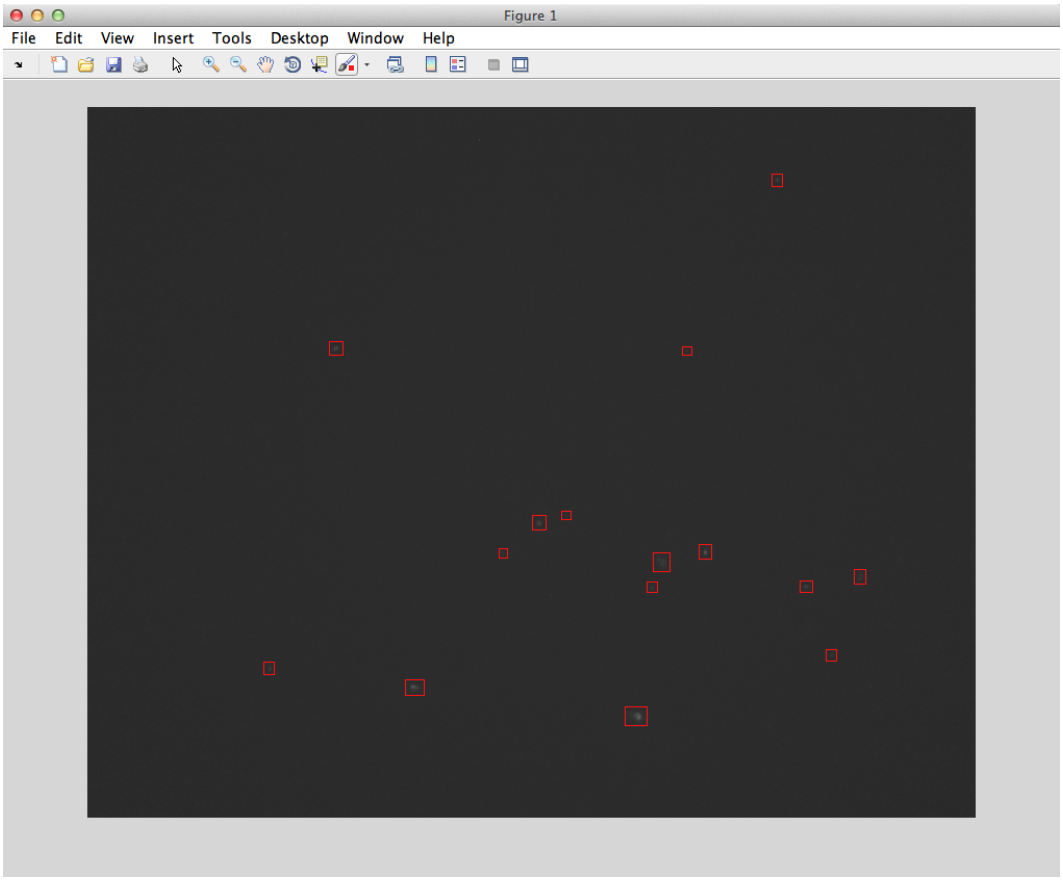

Figure A.3: Particles are detected and data is displayed.

Bibliography

1. D. J. Adams, J. C. Spendlove, R. S. Spendlove, and B. B. Barnett. Aerosol stability of infectious and potentially infectious reovirus particles. *Applied and Environmental Microbiology*, 44(4):903–908, 1982.

2. M. H. Adams. Bacteriophages. *New York: Interscience Publishers*, 1959.

3. I. E. Agranovski, A. S. Safatov, A. I. Borodulin, O. V. Pyankov, V. A. Petrishchenko, A. N. Sergeev, A. P. Agafonov, G. M. Ignatiev, A. A. Sergeev, and V. Agranovski. Inactivation of viruses in bubbling processes utilized for personal bioaerosol monitoring. *Applied and Environmental Microbiology*, 70(12):6963–6967, 2004.

4. I. E. Agranovski, A. S. Safatov, O. V. Pyankov, A. N. Sergeev, A. P. Agafonov, G. M. Ignatiev, E. I. Ryabchikova, A. I. Borodulin, A. A. Sergeev, H. W. Doerr, H. F. Rabenau, and V. Agranovski. Monitoring of viable airborne SARS virus in ambient air. *Atmospheric Environment*, 38(23):3879–3884, 2004.

5. T. G. Akers, S. Bond, and L. J. Goldberg. Effect of temperature and relative humidity on survival of airborne Columbia SK group viruses. *Applied Microbiology*, 14(3):361–364, 1966.

6. T. G. Akers, C. M. Prato, and E. J. Dubovi. Airborne stability of simian virus 40. *Applied Microbiology*, 26(2):146–148, 1973.

7. L. J. Alvarez, P. Thomen, T. Makushok, and D. Chatenay. Propagation of fluorescent viruses in growing plaques. *Biotechnology and Bioengineering*, 96(3):615–621, 2007.

8. A. A. Andersen. New sampler for the collection, sizing, and enumeration of viable airborne particles. *Journal of Bacteriology*, 76(5):471–484, 1958.

9. P. J. Anderson, J. D. Wilson, and C.F. Hiller. Particle size distribution of mainstream tobacco and marijuana smoke. *American Review of Respiratory Disease*, 140:202–205, 1989.

10. J. Atkinson, Y. Chartier, C. L. Pessoa-Silva, P. Jensen, Y. Li, and W.-H. Seto, editors. *Natural ventilation for infection control in health-care settings*. World Health Organization, 2009.

11. R. M. Atlas. *Handbook of microbiological media*, volume 1. CRC press, 2004.

12. J. E. Benbough. The effect of relative humidity on the survival of airborne Semliki Forest virus. *Journal of General Virology*, 4(4):473–477, 1969.

13. R. F. Berendt and E. L. Dorsey. Effect of simulated solar radiation and sodium fluorescein on the recovery of Venezuelan equine encephalomyelitis virus from aerosols. *Applied Microbiology*, 21(3):447–450, 1971.

14. P. S. Brachman, R. Ehrlich, H. F. Eichenwald, V. J. Gabelli, T. W. Kethley, S. H. Madin, J. R. Maltman, G. Middlebrook, J. D. Morton, I. H. Silver, and E. K. Wolfe. Standard sampler for assay of airborne microorganisms. *Science*, 144(3624):1295, 1964.

15. K. Carlson. Appendix: working with bacteriophages: common techniques and methodological approaches. *Bacteriophages: Biology and Applications*, pages 437–494, 2005.

16. C.-W. Chang, D. Sud, and M.-A. Mycek. Fluorescence lifetime imaging microscopy. In Greenfield Sluder and David E Wolf, editors, *Digital Microscopy, 3rd Edition*, volume 81 of *Methods in Cell Biology*, pages 495–524. Academic Press, 2007.

17. M. RJ. Clokie, A. D. Millard, A. V. Letarov, and S. Heaphy. Phages in nature. *Bacteriophage*, 1(1):31–45, 2011.

18. V. M. Corman, I. Eckerle, T. Bleicker, A. Zaki, O. Landt, M. Eschbach-Bludau, S. van Boheemen, R. Gopal, M. Ballhause, T. M. Bestebroer, D. Muth, M. A. Müller, J. F. Drexler, M. Zambon, A. D. Osterhaus, R. M. Fouchier, and C. Drosten. Detection of a novel human coronavirus by real-time reverse-transcription polymerase chain reaction. *Eurosurveillance*, 17(39):20285ii, 2012.

19. S. A. Dee, J. Deen, J. P. Cano, L. Batista, and C. Pijoan. Further evaluation of alternative air-filtration systems for reducing the transmission of Porcine reproductive and respiratory syndrome virus by aerosol. *Canadian Journal of Veterinary Research*, 70(3):168–175, 2006.

20. H. A. Des Voeux. Fog and Smoke. In *Public Health Congress Meeting*, 1905.

21. C. Duchaine. *Notes de cours MCB6003 Bioaérosol et aérobiologie*. Faculté des sciences et de génie, Université Laval, Québec, 2010.

22. D. C. Edelman and J. Barletta. Real-time PCR provides improved detection and titer determination of bacteriophage. *Biotechniques*, 35(2):368–75., 2003.

23. M. A. Elazhary and J. B. Derbyshire. Aerosol stability of bovine parainfluenza type 3 virus. *Canadian Journal of Comparative Medicine*, 43(3):295, 1979.

24. M. A. Elazhary and J. B. Derbyshire. Effect of temperature, relative humidity and medium on the aerosol stability of infectious bovine rhinotracheitis virus. *Canadian Journal of Comparative Medicine*, 43(2):158–167, 1979.

25. I. Y. Espinosa and S. D. Pillai. Impaction-based sampler for detecting male-specific coliphages in bioaerosols. *Journal of Rapid Methods & Automation in Microbiology*, 10(2):117–127, 2002.

26. M. M. Ferris, C. L. Stoffel, T. T. Maurer, and K. L. Rowlen. Quantitative intercomparison of transmission electron microscopy, flow cytometry, and epifluorescence microscopy for nanometric particle analysis. *Analytical Biochemistry*, 304(2):249–256, 2002.

27. L. Gendron, D. Verreault, M. Veillette, S. Moineau, and C. Duchaine. Evaluation of filters for the sampling and quantification of RNA phage aerosols. *Aerosol Science and Technology*, 44(10):893–901, 2010.

28. S. A. Grinshpun, A. Adhikari, C. Li, M. Yermakov, L. Reponen, E. Johansson, and M. Trunov. Inactivation of aerosolized viruses in continuous air flow with axial heating. *Aerosol Science and Technology*, 44(11):1042–1048, 2010.

29. S. Herfst, E. J. A. Schrauwen, M. Linster, S. Chutinimitkul, E. de Wit, V. J. Munster, E. M. Sorrell, T. M. Bestebroer, D. F. Burke, D. J. Smith, G. F. Rimmelzwaan, A. D. M. E. Osterhaus, and R. A. M. Fouchier. Airborne transmission of influenza A/H5N1 virus between ferrets. *Science*, 336(6088):1534–1541, June 2012.

30. J. Hermann, S. Hoff, C. Munoz-Zanzi, K. J. Yoon, M. Roof, A. Burkhardt, and J. Zimmerman. Effect of temperature and relative humidity on the stability of infectious porcine reproductive and respiratory syndrome virus in aerosols. *Veterinary Research*, 38(1):81–93, 2007.

31. W. C. Hinds. *Aerosol Technology : Properties, Behavior and Measurment of Airborne Particles*, chapter 1, pages 1–14. Wiley-Interscience, 1999.

32. Jr. Hogan C. J., E. M. Kettleson, M. H. Lee, B. Ramaswami, L. T. Angenent, and P. Biswas. Sampling methodologies and dosage assessment techniques for submicrometre and ultrafine virus aerosol particles. *Journal of Applied Microbiology*, 99(6):1422–1434, 2005.

33. M. K. Ijaz, S. A. Sattar, T. Alkarmi, F. K. Dar, A. R. Bhatti, and K. M. Elhag. Studies on the survival of aerosolized bovine rotavirus (UK) and a murine rotavirus. *Comparative Immunology Microbiology and Infectious Diseases*, 17(2):91–98, 1994.

34. M. K. Ijaz, S. A. Sattar, C. M. Johnson-Lussenburg, and V. S. Springthorpe. Comparison of the airborne survival of calf rotavirus and poliovirus type 1 (Sabin) aerosolized as a mixture. *Applied and Environmental Microbiology*, 49(2):289–293, 1985.

35. M. K. Ijaz, S. A. Sattar, C. M. Johnson-Lussenburg, V. S. Springthorpe, and R. C. Nair. Effect of relative humidity, atmospheric temperature, and suspending medium on the airborne survival of human rotavirus. *Canadian Journal of Microbiology*, 31(8):681–685, 1985.

36. ISS. Lifetime data of selected fluorophores, http://www.iss.com/resources/reference/data_-tables/LifetimeDataFluorophores.html, page visited on March 10, 2013 .

37. K. Iwasaki, B. L. Trus, P. T. Wingfield, N. Cheng, G. Campusano, V. B. Rao, and A. C. Steven. Molecular architecture of bacteriophage T4 capsid: vertex structure and bimodal binding of the stabilizing accessory protein, Soc. *Virology*, 271(2):321–333, 2000.

38. G. C. Lander, A. Evilevitch, M. Jeembaeva, C. S. Potter, B. Carragher, and J. E. Johnson. Bacteriophage lambda stabilization by auxiliary protein gpD: timing, location, and mechanism of attachment determined by cryo-EM. *Structure*, 16(9):1399–1406, 2008.

39. E. W. Larson, J. W. Dominik, and T. W. Slone. Aerosol stability and respiratory infectivity of japanese B encephalitis virus. *Infection and Immunity*, 30(2):397–401, 1980.

40. J.-H. Lee, C.-Y. Wu, C. N. Lee, D. Anwar, K. M. Wysocki, D. A. Lundgren, S. Farrah, J. Wander, and B. K. Heimbuch. Assessment of iodine-treated filter media for removal and inactivation of MS2 bacteriophage aerosols. *Journal of Applied Microbiology*, 107(6):1912–1923, 2009.

41. X. Li, Q. Liu, X. Bi, G. Sheng, J. Fu, P. Ran, and B. Li. An in vitro model to evaluate virus aerosol characteristics using a GFP-expressing adenovirus. *Journal of Medical Microbiology*, 57(11):1335–1339, 2008.

42. W. G. Lindsley, T. A. Pearce, J. B. Hudnall, K. A. Davis, S. M. Davis, M. A. Fisher, R. Khakoo, J. E. Palmer, K. E. Clark, I. Celik, C. C. Coffey, F. M. Blachere, and D. H. Beezhold. Quantity and size distribution of cough-generated aerosol particles produced by influenza patients during and after illness. *Journal of Occupational and Environmental Hygiene*, 9(7):443–449, 2012.

43. A. C. Lowen, S. Mubareka, J. Steel, and P. Palese. Influenza virus transmission is dependent on relative humidity and temperature. *Plos Pathogens*, 3(10):1470–1476, 2007.

44. B. Luef, T. R. Neu, and P. Peduzzi. Imaging and quantifying virus fluorescence signals on aquatic aggregates: a new method and its implication for aquatic microbial ecology. *FEMS Microbiology Ecology*, 68(3):372–380, 2009.

45. I. M. Mackay, K. E. Arden, and A. Nitsche. Real-time PCR in virology. *Nucleic Acids Research*, 30(6):1292–1305, 2002.

46. T. Maniatis, E. F. Fritsch, and J. Sambrook. *Molecular cloning: a laboratory manual*, volume 545. Cold Spring Harbor Laboratory Cold Spring Harbor, NY, 1982.

47. J. J. McDevitt, K. M. Lai, S. N. Rudnick, E. A. Houseman, M. W. First, and D. K. Milton. Characterization of UVC light sensitivity of vaccinia virus. *Applied and Environmental Microbiology*, 73(18):5760–5766, 2007.

48. J. J. McDevitt, D. K. Milton, S. N. Rudnick, and M. W. First. Inactivation of poxviruses by upper-room UVC light in a simulated hospital room environment. *PLoS ONE*, 3(9):e3186, 2008.

49. T. A. Myatt, S. L. Johnston, S. Rudnick, and D. K. Milton. Airborne rhinovirus detection and effect of ultraviolet irradiation on detection by a semi-nested RT-PCR assay. *BMC Public Health*, 3(http://www.biomedcentral.com/1471–2458/3/5), 2003.

50. M. Oda, M. Morita, H. Unno, and Y. Tanji. Rapid detection of Escherichia coli O157:H7 by using green fluorescent protein-labeled PP01 bacteriophage. *Applied and Environmental Microbiology*, 70(1):527–534, 2004.

51. K. L. Opel, D. Chung, and B. R. McCord. A study of PCR inhibition mechanisms using real time PCR. *Journal of forensic sciences*, 55(1):25–33, 2010.

52. A. C. Ortmann and C. A. Suttle. *Determination of virus abundance by epifluorescence microscopy*, volume 501 of *Methods in Molecular Biology*, pages 87–95. Humana Press, 2009.

53. J. H. Paul, S. C. Jiang, and J. B. Rose. Concentration of viruses and dissolved DNA from aquatic environments by vortex flow filtration. *Applied and Environmental Microbiology*, 57(8):2197–2204, 1991.

54. P. E. Perrott. *Detection of bacteriophage and respiratory viruses in droplets*. PhD thesis, Queensland University of Technology, 2011.

55. L. Qin, A. Fokine, E. O'Donnell, V. B. Rao, and M. G. Rossmann. Structure of the small outer capsid protein, Soc: a clamp for stabilizing capsids of T4-like phages. *Journal of Molecular Biology*, 395(4):728–741, 2010.

56. F. Rabey, R. J. Janssen, and L. M. Kelley. Stability of St. Louis encephalitis virus in the airborne state. *Applied Microbiology*, 18(5):880–882, 1969.

57. C. J. Roy and D. K. Milton. Airborne transmission of communicable infection–the elusive pathway. *New England Journal of Medicine*, 350(17):1710–1712, 2004.

58. W. Rudolph and M. Kempe. Trends in optical biomedical imaging. *Journal of Modern Optics*, 44(9):1617–1642, 1997.

59. M. L. Russell, R. Goth-Goldstein, M. G. Apte, and W. J. Fisk. Method for measuring the size distribution of airborne rhinovirus. *Proceedings of the Indoor Air 2002 Conference, Monterey, CA*, 1:40–45, 2002.

60. S. A. Sattar, M. K. Ijaz, C. M. Johnson-Lussenburg, and V. S. Springthorpe. Effect of relative humidity on the airborne survival of rotavirus SA11. *Applied and Environmental Microbiology*, 47(4):879–881, 1984.

61. F. L. Schaffer, M. E. Soergel, and D. C. Straube. Survival of airborne Influenza virus: effects of propagating host, relative humidity, and composition of spray fluids. *Archives of Virology*, 51:263–273, 1976.

62. M. A. Schoenbaum, J. J. Zimmerman, G. W. Beran, and D. P. Murphy. Survival of pseudorabies virus in aerosol. *American Journal of Veterinary Research*, 51(3):331–333, 1990.

63. A. Shopov, S. C. Williams, and P. G. Verity. Improvements in image analysis and fluorescence microscopy to discriminate and enumerate bacteria and viruses in aquatic samples. *Aquatic Microbial Ecology*, 22(2):103–110, 2000.

64. J. R. Songer. Influence of relative humidity on the survival of some airborne viruses. *Applied Microbiology*, 15(1):35–42, 1967.

65. Z. Tong and Y. Deng. Synthesis of polystyrene encapsulated nanosaponite composite latex via miniemulsion polymerization. *Polymer*, 48(15):4337–4343, 2007.

66. C. C. Tseng and C. S. Li. Collection efficiencies of aerosol samplers for virus-containing aerosols. *Journal of Aerosol Science*, 36(5–6):593–607, 2005.

67. C. C. Tseng and C. S. Li. Ozone for inactivation of aerosolized bacteriophages. *Aerosol Science and Technology*, 40(9):683–689, 2006.

68. N. Turgeon, F. McNicoll, M.-J. Toulouse, A. Liav, J. Barbeau, J. Ho, C. Grund, and C. Duchaine. Neuraminidase activity as a potential enzymatic marker for rapid detection of airborne viruses. *Aerosol Science and Technology*, 45(2):183–195, 2011.

69. S. L. Upton, D. Mark, E. J. Douglass, D. J. Hall, and W. D. Griffiths. A wind tunnel evaluation of the physical sampling efficiencies of three bioaerosol samplers. *Journal of Aerosol Science*, 25(8):1493–1501, 1994.

70. D. Verreault, S. Moineau, and C. Duchaine. Methods for sampling of airborne viruses. *Microbiology and Molecular Biology Reviews*, 72(3):413–444, 2008.

71. D. Verreault, G. M. Rousseau, L. Gendron, D. Massé, S. Moineau, and C. Duchaine. Comparison of polycarbonate and polytetrafluoroethylene filters for sampling of airborne bacteriophages. *Aerosol Science and Technology*, 44(3):203–207, 2010.

72. C. M. Walker and GP. Ko. Effect of ultraviolet germicidal irradiation on viral aerosols. *Environmental Science and Technology*, 41(15):5460–5465, 2007.

73. M. Wang and G. Brion. Effects of RH on glass microfiber filtration efficiency for airborne bacteria and bacteriophage over time. *Aerosol Science and Technology*, 41(8):775–785, 2007.

74. J. C. Warren and M. T. Hatch. Survival of T3 coliphage in varied extracellular environments. I. Viability of the coliphage during storage and in aerosols. *Applied Microbiology*, 17(2):256–261, 1969.

75. K. Wen, A. C. Ortmann, and C. A. Suttle. Accurate estimation of viral abundance by epifluorescence microscopy. *Applied and Environmental Microbiology*, 70(7):3862–3867, 2004.

76. K. Willeke. Method for aerodynamic particle size analysis, patent number US 5949001 A, 1999.